MIDAS

MANAGING IMPACTS OF DEEP SEA RESOURCE EXPLOITATION

Project acronym:	MIDAS
Grant Agreement:	603418
Deliverable number:	Deliverable 2.5
Deliverable title:	Report on variance and persistence of hydrodynamic conditions at three case study sites
Work Package:	WP 2
Date of completion:	12 October 2015

MIDAS MANAGING IMPACTS OF DEEP SEA RESOURCE EXPLOITATION

Report on variance and persistence of hydrodynamic conditions at three case study sites

Deliverable 2.5

Anna Rabitti and Leos R.M. Maas

NIOZ Royal Netherlands Institute for Sea Research,

Department of Physical Oceanography,

P.O. Box 59, 1790 AB Den Burg,

Texel, the Netherlands

12 October 2015

Contents

1. Introduction 2

2. Site 1: Rainbow hydrothermal vent field (MAR) 4

2.1 Data, instruments and methods 4

2.2 Results and discussion 8

3. Site 2: Lucky Strike hydrothermal vent field (MAR) 20

3.1 Data, instruments and methods 21

3.2 Results and discussion 21

4. Site 3: Clarion-Clipperton Zone polymetallic nodule deposits 24

4.1 Measurements around 7º40'N, 134ºW (1972) 25

4.2 Measurements from 12-16ºN, 129-133ºW (1984-1990) 25

4.3 Measurements from the Eastern BGR license area (2013-2014) 26

5. Conclusions and implications for deep-sea mining 28

6. References 29

1. Introduction

The impact of mining activities on deep-sea ecological communities will primarily depend on the techniques adopted for direct seabed disturbance, mining tailings discharge, and for the spatial dilution of the sediment plumes created. All these processes will take place in an extremely complex (and mostly unknown) environment - the deep sea. Site-specific hydrodynamic and hydrographic characteristics will play a key role in shaping the initial behaviour, dilution and horizontal and vertical spreading of the mining discharge. Knowing the background conditions of the surroundings of a mining site is thus paramount in order to understand, predict (via modelling) and mitigate the response of a site to human intervention.

Use of in situ data from the study site is preferable to data from model outputs only, especially where complex topography and/or small scale local dynamics dominate the general current behaviour, such as is the case for hydrothermal vent fields on the Mid Atlantic Ridge (MAR). In those locations, in fact, our modelling skills still fall short. On the other hand, the behaviour of mine tailings discharge will depend on ocean flows at scales of hundreds of metres or less, encompassing turbulent processes down to viscous scales (centimetres and below). Realistically, these scales are impossible to capture with oceanographic sampling, so a combination of in situ data and constrained fine-scale modelling constitutes the ideal tool for gathering background information on a potential mining site.

This report focuses on the variance and persistence of hydrodynamic conditions at three case study sites (see Figure 1), chosen from the many potential mining sites worldwide.

As case studies, we have here considered two diverse types of deep-sea environment:

1. The Mid-Atlantic Ridge (MAR), characterised by high topographic complexity, often with an axial canyon at the spreading centre and transverse canyons on its flanks (Figure 1b). At the MAR, we have considered the Rainbow hydrothermal vent field (Section 2) and the Lucky Strike hydrothermal vent field (Section 3).
2. The Clarion-Clipperton Zone (CCZ) in the Pacific: a relatively flat abyssal plain with isolated and abrupt topographic features (Section 4).

When considering potential deep-sea mining sites and environmental impact, hydrothermal vent fields in all oceans are of particular interest for two main reasons. Firstly, these are the places where mineral-rich (copper, manganese, and rare earth minerals, etc.) deposits are found, and thus present a priority target for mining activities. Secondly, they are natural laboratories for the study of plume dispersion in the deep sea in very complex topographic settings (Figure 2a). In fact, high-temperature (300º C) vent fields give rise to particle-rich plumes rising hundreds of meters above the seafloor, where they spread laterally into the surrounding water column. Understanding the behaviour of natural plumes can help in understanding the future behaviour of artificial plumes produced by mining activities. We know that natural hydrothermal plumes support unique and fascinating ecosystems, and play a key role in the dispersal of larvae and chemicals, but we are very uncertain about the potential consequences of artificial sediment plumes that could be produced in the same environment.

Abyssal plains rich in manganese nodules such as the CCZ are also of interest as target mining sites (Figure 2b). Regarding the behaviour of artificial plumes in abyssal plain settings, we can hypothesize that modelling would be simpler here because of the relatively flat topography. However, local hydrodynamic and hydrographic conditions and their temporal and spatial variability are also of great importance when predicting the vertical and lateral spreading of the tailings.

For the sites on the MAR (sections 2 and 3) we will present new in situ data, acquired within the MIDAS project during two oceanographic campaigns in May 2014 (cruise 64PE388, RV Pelagia) and

April 2015 (cruise 64PE398, RV Pelagia). For the Rainbow site, we will also present time series of hydrodynamic data. For the CCZ site (Section 4), a literature review will be used for the characterisation.

Our focus is on the site-specific conditions that have implications and possibly interactions with mining activities. For details on the relevant deep ocean processes, see Dale and Inall (2015) and Rabitti and Maas (2015). From an observational point of view, this means that data come from the vicinity (***O*** (10) m - ***O*** (10) km) of the possible source, and mainly from the lower part of the water column, since the near-bottom environment is of particular interest in this context.

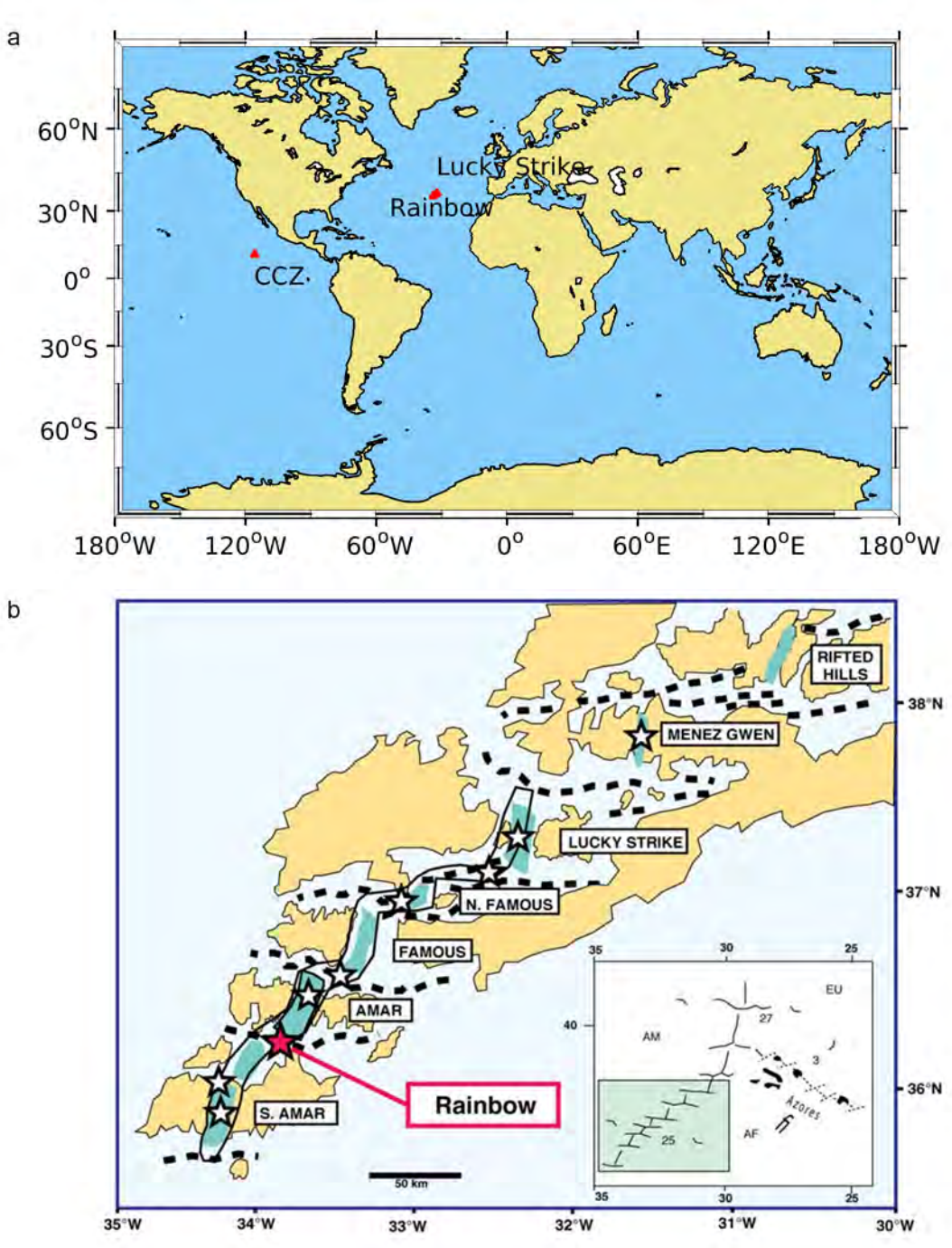

Figure 1 (previous page): a) The three case study sites: Lucky Strike and Rainbow hydrothermal vent fields almost overlap on the Mid Atlantic Ridge, and the Clarion-Clipperton Zone (CCZ) in the Pacific. b) The MAR,

south-west of the Azores Triple junction. Among others, the Lucky Strike and Rainbow hydrothermal vent fields are marked. In the inlet, its position with respect to the Azores is indicated (figure from German et al., 2010).

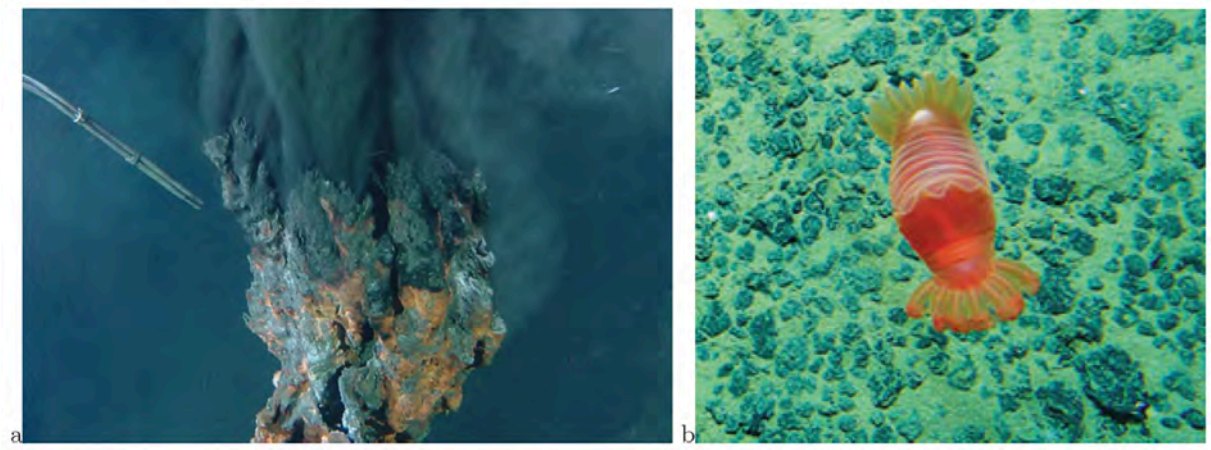

*Figure 2 a) Black Smoker from the Rainbow hydrothermal field (Image courtesy Prof. Fernando J.A.S. Barriga). b) A brightly coloured Holothurian (*Peniagone *sp.) amongst nodules in the Clarion Clipperton Zone (Image courtesy BGR, Bundesanstalt für Geowissenschaften und Rohstoffe).*

2. Site 1: Rainbow hydrothermal vent field (MAR)

The Rainbow hydrothermal plume was discovered during a geophysical survey along 200 km of the MAR in 1996 (German et al., 1996b) and it is the strongest - in terms of plume spatial spreading - of the several hydrothermally active sites discovered during that survey. The Rainbow hydrothermal vent field is located at 33º 54.12' W, 36º 13.78'N, to the SW of the Azores Triple Junction and approximately 20 nautical miles outside the Portuguese Exclusive Economic Zone (EEZ) (Figure 1b). The field is at an average depth of 2300 m and comprises about ten high-temperature (365º C) vents (Dymant et al., 2009; German et al., 2010).

The key literature references for this site are: Aleynik and Lukashin, 2005; Cave et al., 2002; Dymant et al., 2009; German et al., 1996b, 1998, 2010; Thurnherr, 2006; Thurnherr and Richards, 2001; Thurnherr et al., 2002.

2.1 Data, instruments and methods

The dataset presented in this report was collected during two multi-disciplinary cruises (64PE388 in May 2014 and 64PE398 in April 2015) with RV Pelagia in the Rainbow field area, combining the scientific goals of the Treasure (Dutch) and MIDAS (European) projects. The Treasure team focused on geological and biological aspects of the area (Figure 3), while the MIDAS team focused on its hydrographic and hydrodynamic characterisation. The MIDAS goals have been achieved using a variety of instruments.

Figure 3: Snapshots from a visual investigation of the surroundings of the Rainbow hydrothermal vent field, May 2014. Images courtesy of M. Lavaleye and L. Klunder, NIOZ Biology Department.

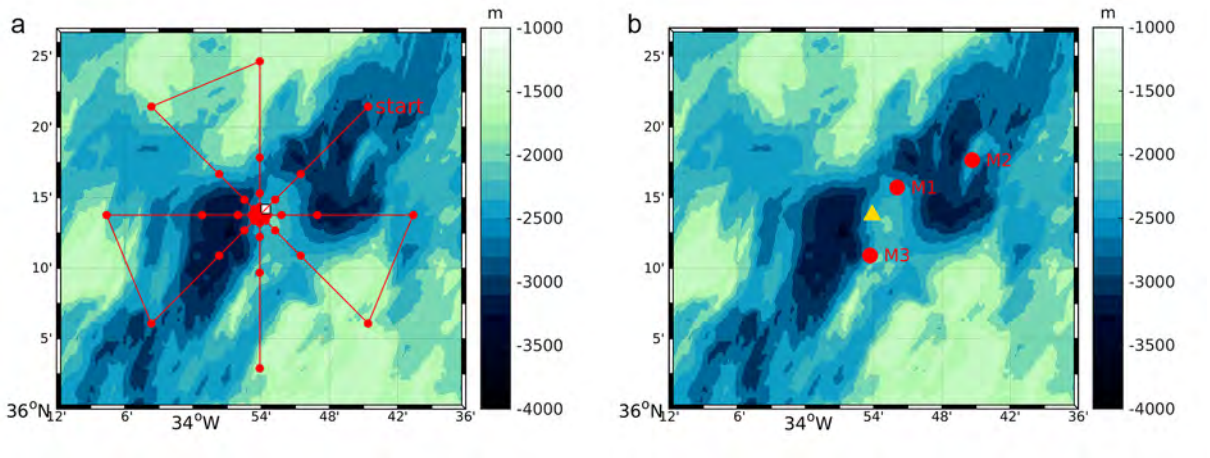

Figure 4: Bathymetric map of the Rainbow area. a) Locations of the 41 CTD/LADCP stations, marked in red. First station is marked as "start" and the ship track is marked in thin red line. On top of the vent field, two more series (circles) of measurements superpose in the figure, one station was also performed on top of the vent, at the end of the series. The white square indicates the position of the 13 h of continuous CTD/LADCP measurements. b) Locations of the three long-term oceanographic moorings M1, M2 and M3 are marked in red. The hydrothermal vent field is marked with the yellow triangle.

During the 2014 cruise, an intense hydrographic and hydrodynamic survey was performed, comprising about 40 stations arranged in a telescopic set of circles, centred on the Rainbow field (see Figure 4a). The radial distance from the vent area of each circle of stations is: 0.5 km, 1.3 km, 3.5 km, 9.4 km and 25 km respectively. At each station, a Sea Bird 911-plus CTD profile was acquired, measuring the classic conductivity-temperature-depth, but also turbidity, fluorescence and oxygen content. After post-processing, all profiles have a vertical resolution of 1 m, with a range between about 5 m below the surface to 20 m above the bottom: a conservative choice due to the bottom roughness of the sampled area. In 2014, the CTD rosette was also equipped with an LADCP (Lowered Acoustic Doppler Current Profiler). The system consists of two 300 kHz TRDI WorkHorse Broadband ADCPs in a master/slave configuration, downward and upward looking respectively, and the battery pack. This setting gives a velocity profile over a maximum of two times 120 m in fifteen 8m-bins in waters with ample scatterers and about two times 60 m in clearer waters. Acquired data were then processed using the velocity inversion method developed at Lamont-Doherty Earth Observatory (LDEO) by M. Visbeck and now maintained by A. M. Thurnherr, Version IX.10, which combines LADCP measurements with CTD and

NMEA (National Marine Electronics Association, a standard for GPS and navigational data) information to improve the quality of the current estimates. All stations present a qualitatively similar error profile, with fairly constant error values throughout the whole water column, and a general increase in the last few tens of meters before the bottom. Error values are in general between 0.03 m/s to 0.05 m/s, with higher values at some of the stations but with no particular relation with the topographic surroundings, the depth, the scatter distribution or the measurement timing. We decided to include results from these stations since the instrument, data acquisition and processing have always been the same, and we cannot detect a particular trend of data quality declining over time.

To further improve the quality of the LADCP data, shipborne velocity measurements were also acquired when profiling, and will be embedded in future analysis. The vessel mounted ADCP (VMADCP) consisted of a 75kHz TRDI Long Ranger ADCP mounted 4 m below the sea surface on the ship hull and operated via VmDas software version 1.46.5. Measurements were acquired in 60 bins of 10 m vertical resolution, covering the first 600 m of the water column.

In addition to the single CTD/LADCP stations, in 2014 a 13-h station was also been performed (white square in Figure 4a), located north-east of the Rainbow field, to assess the hydrographic and hydrodynamic variability of the area on a tidal time scale. The whole water column was sampled in the 10 acquired profiles.

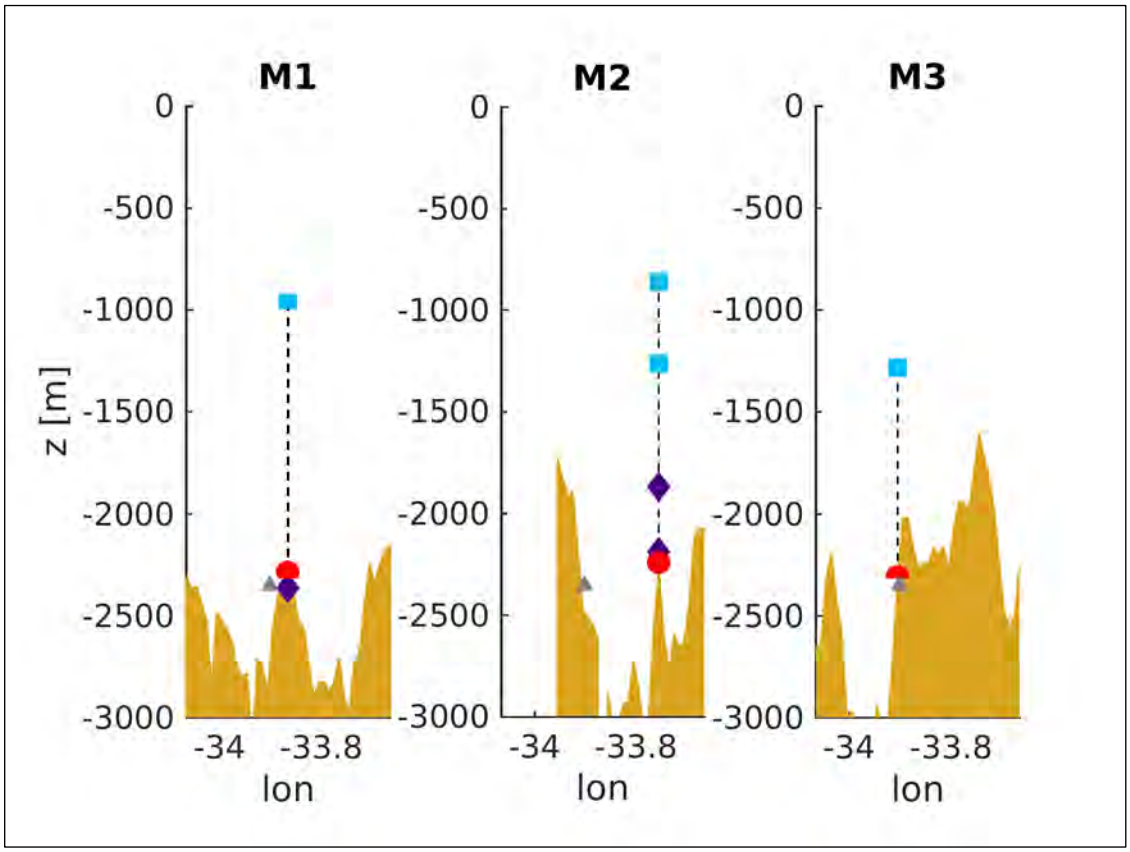

Figure 5: Schematic of instrument positions on the three mooring lines (see Figure 4b for locations). Longitude and depth of Rainbow field is marked with the grey triangle. Red dots represent ADCPs. MicroCats are marked with purple diamonds, while current meters are marked with blue squares.

In 2014, three oceanographic moorings were deployed in the vicinity of the Rainbow vent field in order to monitor the current velocity field and hydrographic properties in the bottom part of the water column at three different locations: in the near field, downstream and upstream of the plume injection, and in

the far field, downstream of the field (see Figure 4b). All three long-term moorings were successfully recovered during the 2015 cruise with no loss of instrumentation, though unfortunately we did experience some instrument failure. The design of the three moorings is sketched in Figure 5, depicting only well-functioning instrumentation. Details on positioning are given in Table 1. In tables 2, 3 and 4, a summary of the data obtained from each mooring is presented.

In short, all three moorings consisted of a bottom, upward-looking 75kHz TRDI Long Ranger ADCP. ADCP data were collected in 74 bins of 8 m vertical resolution, approximately between 2300 m and 1700 m, with an ensemble averaging period of 1200 s (20 min, 29 ping/ensemble), and average error in current speed of 0.03 m/s per ensemble. While the ADCP's batteries were emptying, reliability on the farthest bins was lost and their data has been discarded. Above the ADCP, each mooring was equipped with Nortek AquaDopp or Aanderaa RCM-11 current meters for hydrodynamic measurements, and with SBE 37-SM MicroCats for hydrographic time series, according to Figure 5. For details on instrument depth and record length see tables 2, 3 and 4. The sampling rate for current meters and MicroCats was 600 s (10 min).

In this work, spectra of time series are obtained using the multitaper method, with three discrete prolate spheroidal sequences as data tapers for the multitaper estimation (Percival, 1993; Thomson, 1982). Wavelet analysis is performed following Torrence and Compo (1998).

	Latitude (dec deg)	Longitude (dec deg)	Expected depth (m)
M1	36.2618	-33.8656	2287
M2	36.2942	-33.7554	2267
M3	36.1816	-33.9050	2301

Table 1: Mooring locations (see Figure 4b)

M1 instrument	Mean depth (m)	Start	Stop
microCAT	2330	22-May-2014 21:26:35	07-Apr-2015 10:56:35
ADCP	2344	23-May-2014 21:50:47	10-Nov-2014 09:50:47
NIOZ-hst	2344	March 2014	May 2015
AquaDopp	965	23-May-2014 21:45:44	07-Dec-2014 06:53:22

Table 2: Details for M1, near-field, north-east of plume source; see Figure 5, left panel

M2 instrument	Mean depth (m)	Start	Stop
ADCP	2275	23-May-2014 21:52:10	18-Mar-2015 05:52:10
NIOZ-hst	2275	March 2014	May 2015
microCAT	2216	22-May-2014 21:26:04	08-Apr-2015 16:11:04
microCAT	1890	22-May-2014 21:20:15	08-Apr-2015 16:55:15
AquaDopp	1262	23-May-2014 21:39:10	11-Dec-2014 05:58:52
AquaDopp	860	23-May-2014 21:42:29	06-Dec-2014 21:43:15

Table 3: Details for M2, far-field, north-east of plume source; see Figure 5, central panel

M3 instrument	Mean depth (m)	Start	Stop
ADCP	2340	24-May-2014 17:18:03	23-Mar-2015 05:58:03
NIOZ-hst	2340	March 2014	May 2015
Aanderaa	1283	24-May-2014 15:47:00	10-Apr-2015 14:49:00

Table 4: Details for M3, near-field, south of plume source; see Figure 5, right panel.

2.2 Results and discussion

2.2.1 Spatial variability of currents during May 2014

Current measurements from the CTD/LADCP scheme in Figure 4a are presented in Figure 6 (left panels) for four depth layers: 1000-1500m, 1500-2000m, 2000-2300m (depth of Rainbow plume injection) and 2300m to bottom. It took approximately one week to complete the CTD/LADCP sampling scheme in Figure 4a, and so it follows that the different current profiles were acquired at different times. For this reason, the tide model FES2012 (Carrére et al., 2012) has been used to produce the local barotropic tide prediction at the time of sampling of each station. FES2012 is distributed as an auxiliary AVISO product. It provides global, hydrodynamic non-linear 32-constituents tide solutions (FES - Finite Element Solution) and takes advantage of the most recent altimeter time series, modelling and data assimilation techniques, and accurate ocean bathymetry. Tidal predictions obtained using TPXO7.2 global dataset and OSU inverse tidal model (Egbert and Erofeeva, 2002) for the station locations have also been considered, with similar results.

We notice that the barotropic tidal ellipses in the area, both obtained with FES2012 and with OSU TPO7.2 are, in practice, spatially homogeneous and do not account for the complex local topography, mainly due to their poor horizontal resolution. Recent modelling efforts (Aleynik et al., 2015) have shown that if the high resolution MITgcm model is used (Marshall et al., 1997a,b) and specifically applied to the Rainbow area, the model is capable of capturing some of the effects of topographic features on barotropic tides, giving rise to spatially diverse tidal ellipses (Figure 6a of Aleynik et al., 2015). While the size of the ellipses is comparable among all model outputs (and comparable to the measured values), strong differences in phase between MITgcm results and LADCP measurements are still observed, which is why these high-resolution model results are not used to adjust the observations. This difference in phase, however, suggests the presence of vertically propagating

internal waves, which has possibly led to a shift in the phase of near-bottom currents. Further investigation, for example a vertical mode analysis of the LADCP profiles, would certainly shed some light on this topic. Moreover, information on local tidal (and, in general, temporal) variability is also crucial to be able to estimate a de-tided map of the current velocities in this complex area. We will come back to this issue in the next two sections.

For the moment, we can regard the right panels of Figure 6 as snapshots of the de-tided local currents plus the tidal baroclinic component only. As a general comment, velocity magnitudes do not dramatically decrease below 1500 m to the bottom. Instead, we observe some local bottom enhancements, with measurements of near-bottom velocities exceeding 5 cm/s. These relatively high near-bottom velocities and the likely presence of an extremely active internal wave field are not surprising in such a topographically complex area, where conversion from barotropic to baroclinic tidal motion is expected to happen at the steep flanks of the Rainbow hill and at the lateral walls of the canyon, and may well be accompanied by bottom current intensification (Maas and Zimmerman, 1989).

Although not surprising, these observations should alert future modellers and interested parties to the strong influence of the topography on the local hydrodynamic field, and to the possible consequences that vertically propagating internal waves can have on both horizontal and vertical spreading of an hypothetically injected plume in the area. Estimations of stratification strength and of vertical diffusivity, based on Thorpe scales (Thorpe, 1977) from CTD data acquired in the area, will quantify the local mixing properties and their spatial variability.

From the maps in Figure 6, the near-bottom flow appears to be completely controlled by the topography, especially in the vicinity of the Rainbow hill. The current goes northward along the western flank (see panels 6f and 6h, along the flank), while it recirculates in the pit east of the Rainbow hill (see panel 6h, eastward arrow in the deepest part of the pit). While some of this topographic steering is also observed up in the 1500-2000 layer, it is completely lost in shallower layers (not shown). This behaviour was already observed in Thurnherr and Richards (2001) and Thurnherr et al. (2002) (their sketch of Rainbow mean flow is shown later in Section 2.2.3, Figure 14b), with isolated LADCP profiles and short current meter time series in the area, but now the spatial resolution of the measurements is higher; moreover, with the analysis of the newly acquired, long time series in Section 2.2.3, we will see that this is truly a permanent feature of the Rainbow flow regime.

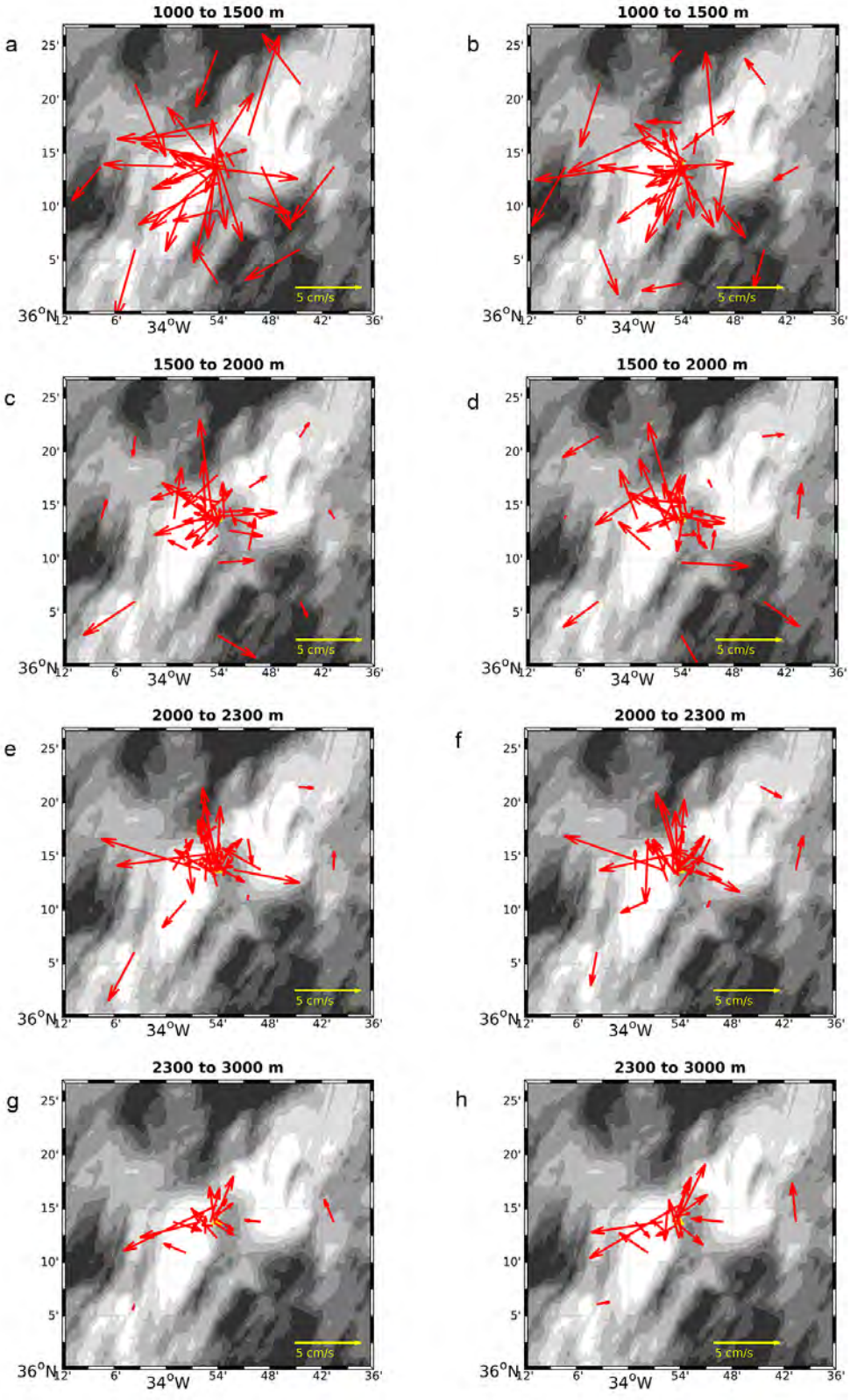

Figure 6: (left) Measured current for each station, from top to bottom: between 1000 and 1500 m, 1500 and 2000 m, 2000 and 2300 m, and 2300 m to bottom. (right) Same as left, but here the modelled barotropic tide has been removed at each station. Tidal predictions are obtained using the FES2012 model (Carrére et al., 2012). Domain and bathymetry are the same as in Figure 4, white colour corresponds to deep areas, black to shallow areas.

2.2.2 Tidal variability of currents

Local tidal variability has been assessed thanks to a 13-hour CTD/LADCP yo-yo station (10 casts in total). The hydrographic and current measurements were performed at about 1.3 km north-east of the Rainbow field on the western flank of the Rainbow hill, between approximately 5 m from the surface to 20 m above the bottom, at about 2250 m. Measured current speed and direction, averaged in four depth layers (1000-1500 m, 1500-1750 m, 1750-2000 m, 2000 m to bottom) are presented in Figure 7. The colour of the arrows represents time, and goes from red to yellow. The first cast started on 18 May 2014, 19:47 UTC, last cast started on 19 May 2014, 07:04 UTC. A thin, black arrow is superimposed on the colour arrow if the particle plume originated by the Rainbow hydrothermal vent field was also observed. The plume was detected thanks to the turbidity measurements made at the same time with a Wet Labs, ECO-NTU sensor mounted on the CTD frame. In the bottom panel of Figure 7, the local barotropic tidal ellipse is shown, as obtained using the FES2012 model (Carrére et al., 2012) for the same time frame. Time colour code is the same as in the other panels.

For the shallower depth layer considered here (1000-1500 m) down to 2000 m, measured current values approximately follow the expected barotropic tidal ellipse. However, absolute values are sometimes three times higher than modelled, barotropic currents. This suggests a strong baroclinic component in the velocity field, which could also account for the shift in phase that is observed in different layers. In the near bottom layer, the tidal ellipse collapses due to the topographic steering of the currents. In fact, here we never observe south-westerly flow, and instead the current is always directed north, north-east, or - as at the beginning of the 13-hour series of measurements - south-east, in a cross-channel direction. Below 2000 m, tidal effects are thus confirmed to be weak compared to hydraulically controlled flow, as observed during the 10-hour measurements reported in Thurnherr and Richards (2001). The shift in phase from the model results (Figure 7e) is greater than at other depths, again pointing at the possible presence of vertically propagating internal waves, most likely resulting from processes of conversion between barotropic to baroclinic tide due to the interactions with the local topography. The phase of isopycnal displacement has been already observed to vary over time at tidal timescales (Thurnherr and Richards, 2001), confirming our results. Even in this near-bottom layer, measured current magnitudes are sometimes two or three times the expected barotropic tidal current, especially when the flow is parallel to the local topography. Bottom enhancement of currents is thus happening periodically within a tidal circle, but although it seems to happen when the flow is directed along the isobaths of the Rainbow hill it does not happen every time - see for example the small velocities measured at the beginning of the series of measurements. The occurrence of these local, near-bottom phenomena (current enhancement, strong topographic steering, tidal phase shift as an indication of vertically propagating internal waves) are of particular relevance if one is interested in the behaviour of a natural or artificial plume released in the area since they could interact, shape and/or control the horizontal and vertical dispersion of particles and tailings material in the near field as well as in the far field of the plume source.

The presence or absence of the Rainbow hydrothermal plume, detected by optical turbidity measurements performed at the same time as the velocity measurements, is very informative but puzzling. Though the current direction is not dramatically changing throughout the 13 h in this near-bottom layer (implying the presence of a strong topographically steered rectified current), strong time variability in the presence of the plume is observed (see presence or absence of thin, black arrow within the corresponding colour coded arrow). We exclude the changing strength of the current as possible explanation for this plume variability. The plume is detected or not despite the magnitude of the measured velocities being more or less strong. It simply seems that the plume was not there for the first 3 casts of the series, until about midnight, but it was always detected in the subsequent profiles. We cannot exclude variability of the plume emission itself, but we have no measurements to confirm or reject this hypothesis. Moreover, it was also noted in Thurnherr and Richards (2001) that in the stations closest to the Rainbow vent field, both the horizontal and the vertical variability of the

plume (detected via optical turbidity measurements) was the highest, in accordance to observations at other hydrothermal sites.

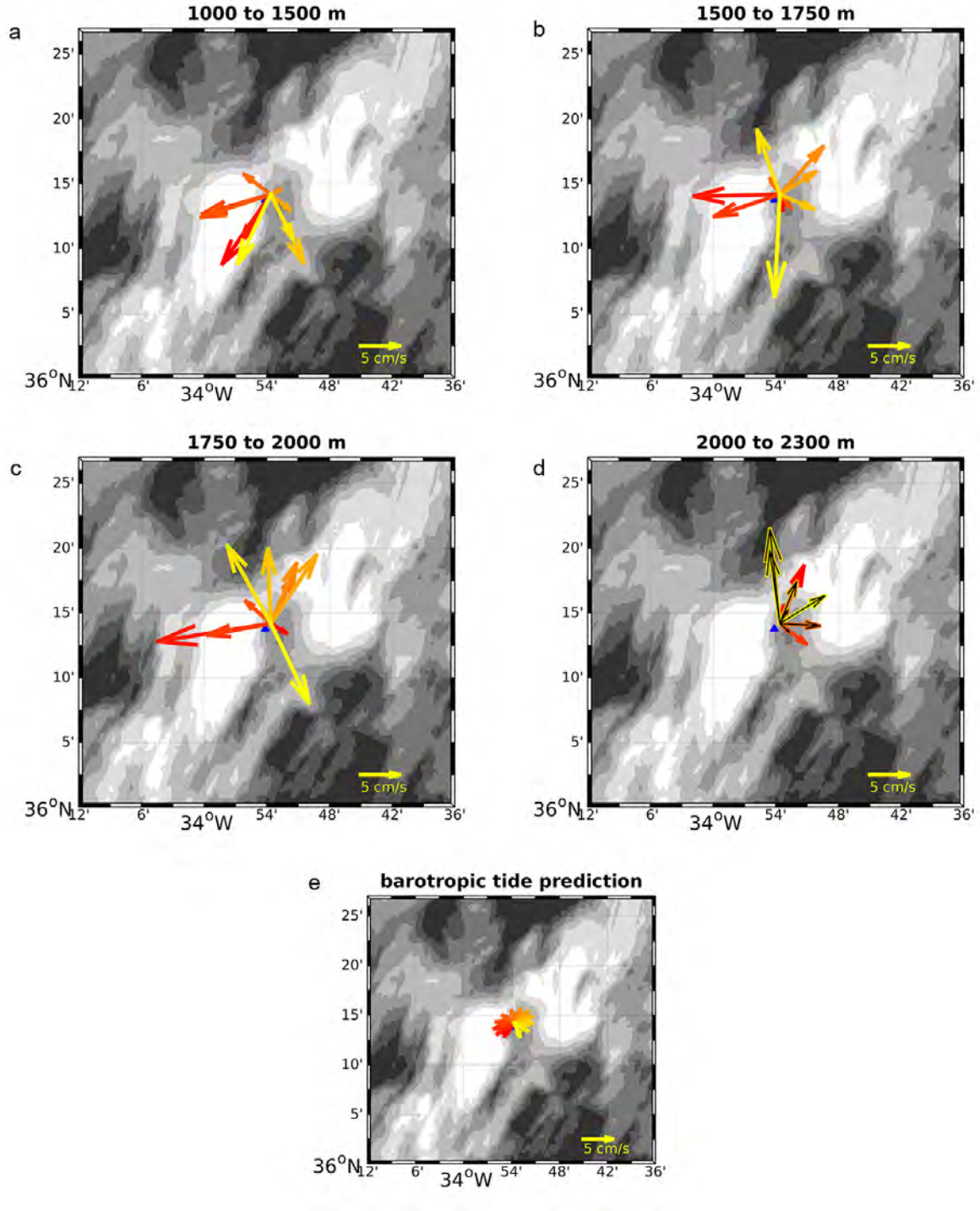

Figure 7 a-d) Top to bottom, left to right, current speed and direction as measured by the LADCP averaged in four depth layers, according to each panel legend. Colour of the arrows represents time, from red to yellow. First cast started on the 18th of May 2014, 19:47 UTC, last cast started on the 19th of May 2014, 07:04 UTC. A thin black arrow is superposed on the colour arrow when the plume is detected using turbidity measurements. e) The local barotropic tidal ellipse as obtained using the FES2012 model (Carrére et al., 2012) for the same time frame. Time colour code is the same as in the other panels. The blue triangle marks the position of the Rainbow vent field. Domain and bathymetry are the same as in Figure 4.

2.2.3 Long-term variability of currents

a) Time series

Measurements from the long-term moorings (see Figure 4b) are presented in this section. Raw near-bottom, zonal and meridional currents from ADCPs are displayed in Figure 8. Note that duration of the measurements at M1 (Figure 8a and b) is shorter than in the other two locations. Note also that the colour scale for the M1 zonal current component is different to account for the local, stronger current values. This is explained if we consider the location of M1, on the northern tip of the Rainbow hill. As we have also seen in the 13h yo-yo measurements (Figure 7), the flow at this position is mainly zonal, and directed eastward, following the topographic contours around the Rainbow hill.

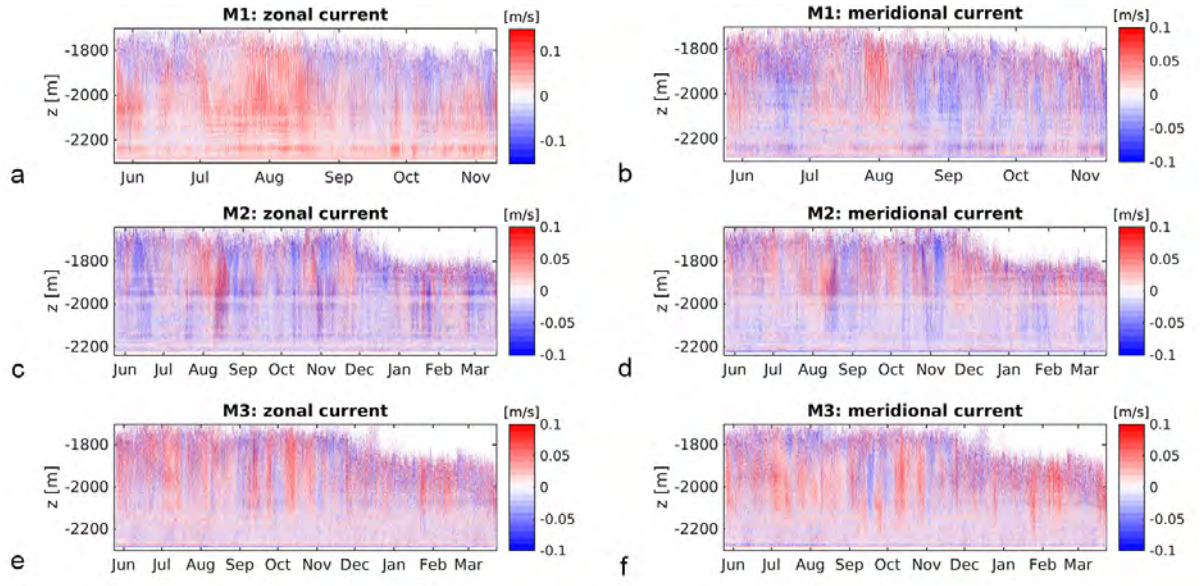

Figure 8: Raw measurements of zonal (left) and meridional (right) currents from the three moored near-bottom ADCPs. Time goes from May 2014 to December 2014 for M1, and from May 2014 to April 2015 for M2 and M3. Ticks denote the beginning of the month. The number of bins reduces in time as the battery power drains. Note that colour scale is different for the M1 zonal component.

Measurements from the shallower current meters (see Figure 5 for mooring designs) are presented in Figure 9. Here, time goes from May 2014 to December 2014 for M1 and M2 (9a to f), and from May 2014 to April 2015 for M3 (9g and h), reflecting battery performances. Thin, light lines show all available measurements, with a sampling interval of 10 minutes. Thicker, dark lines correspond to a 25h-moving average of the signals, smoothing out the high frequency, tidal variability. At the three locations, zonal and meridional components of the current present similar velocity magnitudes at all depths throughout the whole time series. Only a few strong current events are recorded, revealing a peculiar correlation among the three mooring locations. For example, in November 2014 one event stands out in two out of four current meter measurements: a strong southward current is measured both by M1 and by M2 in November 2014, but only above 1000 m. The same signal is measured at two different locations (M1 and M2), approximately 10 km apart, in the same depth layer (965 m and 860 m respectively), whilst at location (M2), at the same time, the strong signature is lost at 400 m below (at 1260 m). Moreover, such a strong, southward current is not accompanied by any notable event in the zonal velocity component.

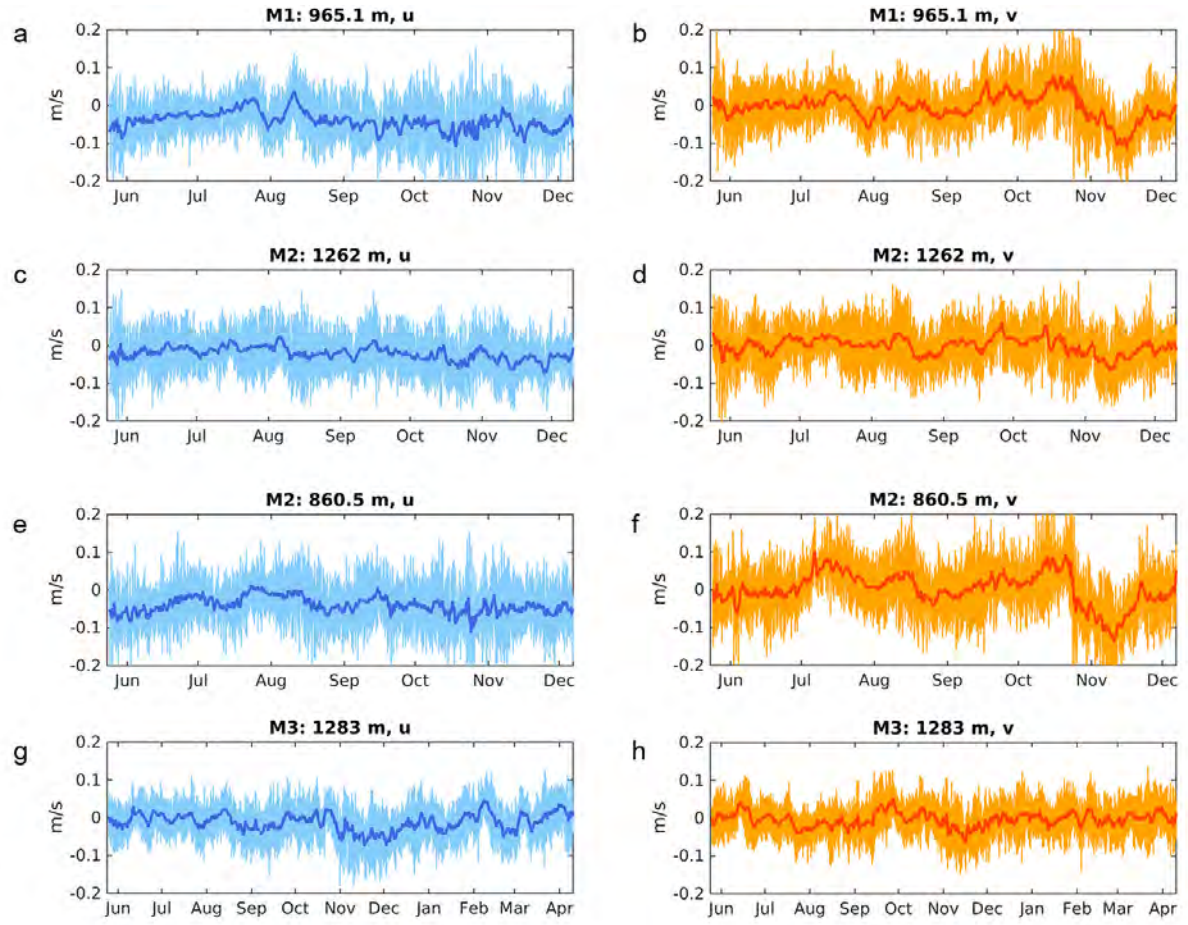

Figure 9: Measurements of zonal (left) and meridional (right) currents from the four moored current meters. Time goes from May 2014 to December 2014 for M1 and M2, and from May 2014 to April 2015 for M3. Thin light lines show all measurements. Thicker, darker lines correspond to a 25h-moving average of the signals.

This suggests that in the Rainbow area hydrodynamics is very distinct in different depth layers. This was already observed for deeper layers, where a distinct dynamic was measured above and below the 2000 m (Thurnherr and Richards, 2001). With these new measurements, we can also clearly distinguish between a dynamic above and below 1000 m. For the moment, we can only speculate on the origin of the event in the depth layer above 1000 m. There are two possible mechanisms for such a strong southward current south-west of the Azores: i) an atmospheric storm, or ii) the passage of a Mediterranean eddy (meddy). Meddies are warm and salty eddies of Mediterranean water, sinking in the northeast Atlantic through the Gibraltar Strait. Meddies play an important role in maintaining the temperature and salinity distributions in the North Atlantic, but relatively little is known about their early life histories, including where, how often and by what mechanism they form. Unfortunately, we do not have hydrographic information at the same depth for that period from the moorings (see Figure 5); further investigation is thus needed using other available data sets (wind maps to check for storm presence, satellite sea level anomaly or ARGO temperature and salinity data to check for meddy passage).

b) Spectral analysis

Spectral analysis of ADCP and current meter data allows for better hydrodynamic characterisation of the area and its variability at different timescales. The whole spectrum for ADCP's measurements is presented in Figure 10, for the zonal (left) and meridional (right) component. Each line corresponds to

the average of 5 bins, centred at the depths reported in the legend. Black vertical lines mark the main tidal components, while the dashed vertical line corresponds to the local inertial frequency f ($f = 2\Omega \sin \phi$, where Ω is the Earth rotation rate and ϕ the local latitude). Periods range from 128 (256) days for M1 (M2 and M3) to 45 minutes (1= 32 of a day). According to typical values for the buoyancy frequency N ($10^{-4}\ s^{-1}$ below 2000 m; Thurnherr and Richards, 2001), the full internal wave window is then covered by these current measurements. In Figure 11, a zoom between 9 to 29 h is shown. This is done to appreciate the spectral behaviour of the two components of the current in this period window, relevant for tidal variability.

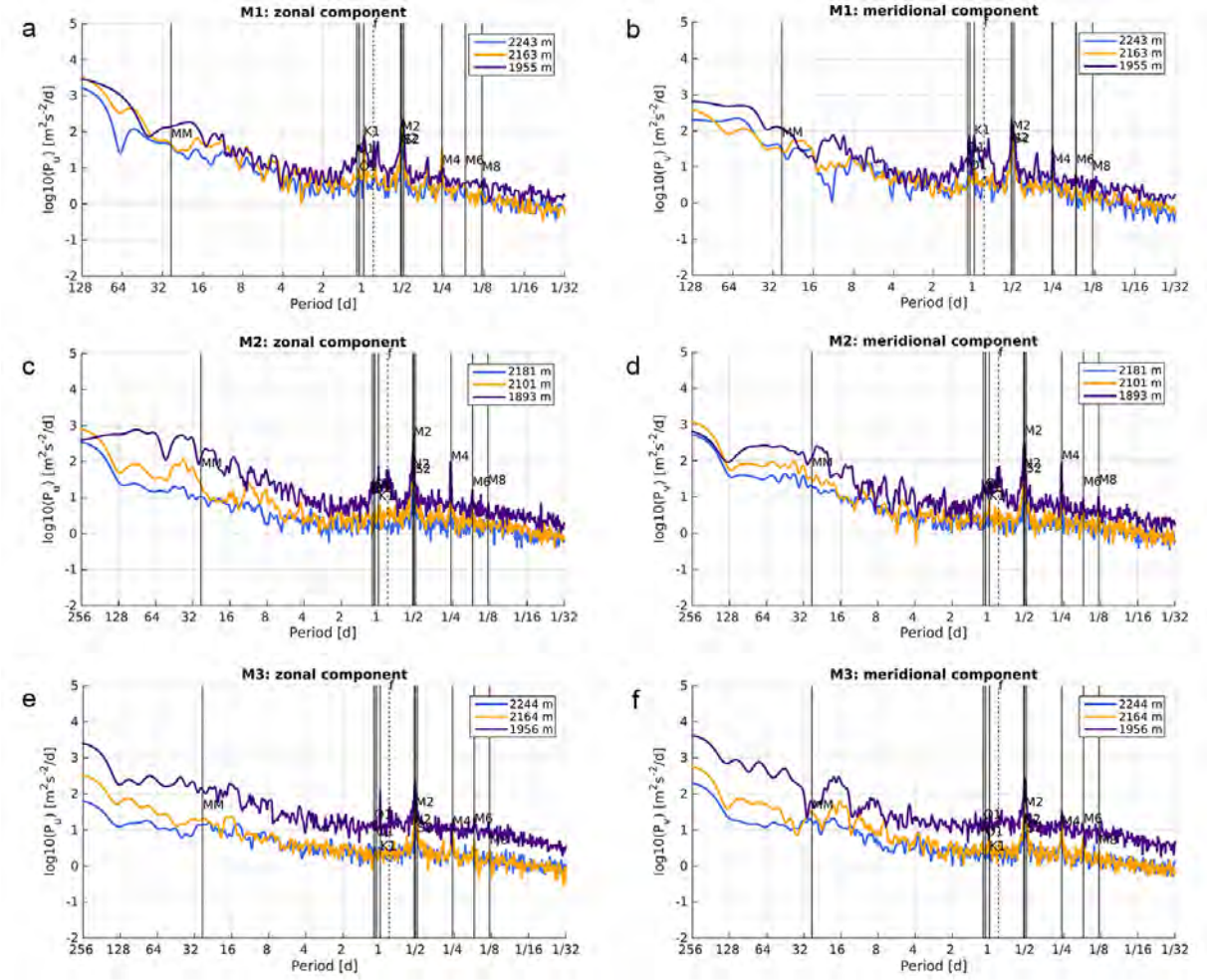

Figure 10: Spectral analysis for the zonal (left) and meridional (right) current components. Each line corresponds to the average of 5 bins, centred at the depths reported in the legend. Black vertical lines mark the main tidal components, while the dashed vertical line corresponds to the local inertial frequency. Periods go from 128 (256) days for M1 (M2 and M3) to 45 minutes (1=32 of a day).

Indeed, zonal velocities at M1 are the most energetic amongst all the other measurements for the three depths, as already observed in Figure 8. If we instead consider only the shallowest depth (around 1950 m), both zonal and meridional components at M3 prevail, with their power quickly diminishing towards the bottom. If we look at the shallow depth, similar peaks at about 15 d and 28 d are present with different strengths at all locations. It is also worth noticing that no peaks are observed in the near-bottom bins in the slower part of the spectra. It seems that low frequency features are mainly affecting the shallower depths, while the near-bottom depth is dominated by relatively high frequency peaks. This leads to a special interest in the tidal period (Figure 11), and this reveals some interesting aspects of near-bottom dynamics. First, inertial peaks are dominant only above 2000 m.

Below this depth, little to no signature of near-inertial frequency is found. This is confirmed from the current meter measurements (Figure 12), where instead a strong signature of near-inertial waves is found at all locations. We can thus hypothesize that these near-inertial waves are triggered at the surface by near-inertial wind stress, and are able to travel obliquely at great depths without reaching the bottom, where dynamics appear more tidally dominated. In fact, at M1, we observe a strong, unexpected near-bottom enhancement of the K1 tidal component, that in the zonal velocity reaches and even exceeds the M2 and S2 tidal components. This is possible since the K1 tidal component is subinertial in this region (see Figure 11a), and is thus prone to trapping by the topography, while super inertial waves (as for example the M2 and S2 tidal components) cannot be trapped. It follows that this is a local effect, but for its positioning in the vicinity of the Rainbow hydrothermal plume source, it may have big consequences on the spreading pattern of the plume particles. If, in the near-bottom layer, a diurnal variability prevails over a semidiurnal variability, this may have also affected the 13 h measurements performed not far from M1 mooring location, and should be taken into consideration if one is interested in the near-field dynamics of the vent field in such a topographically complex environment.

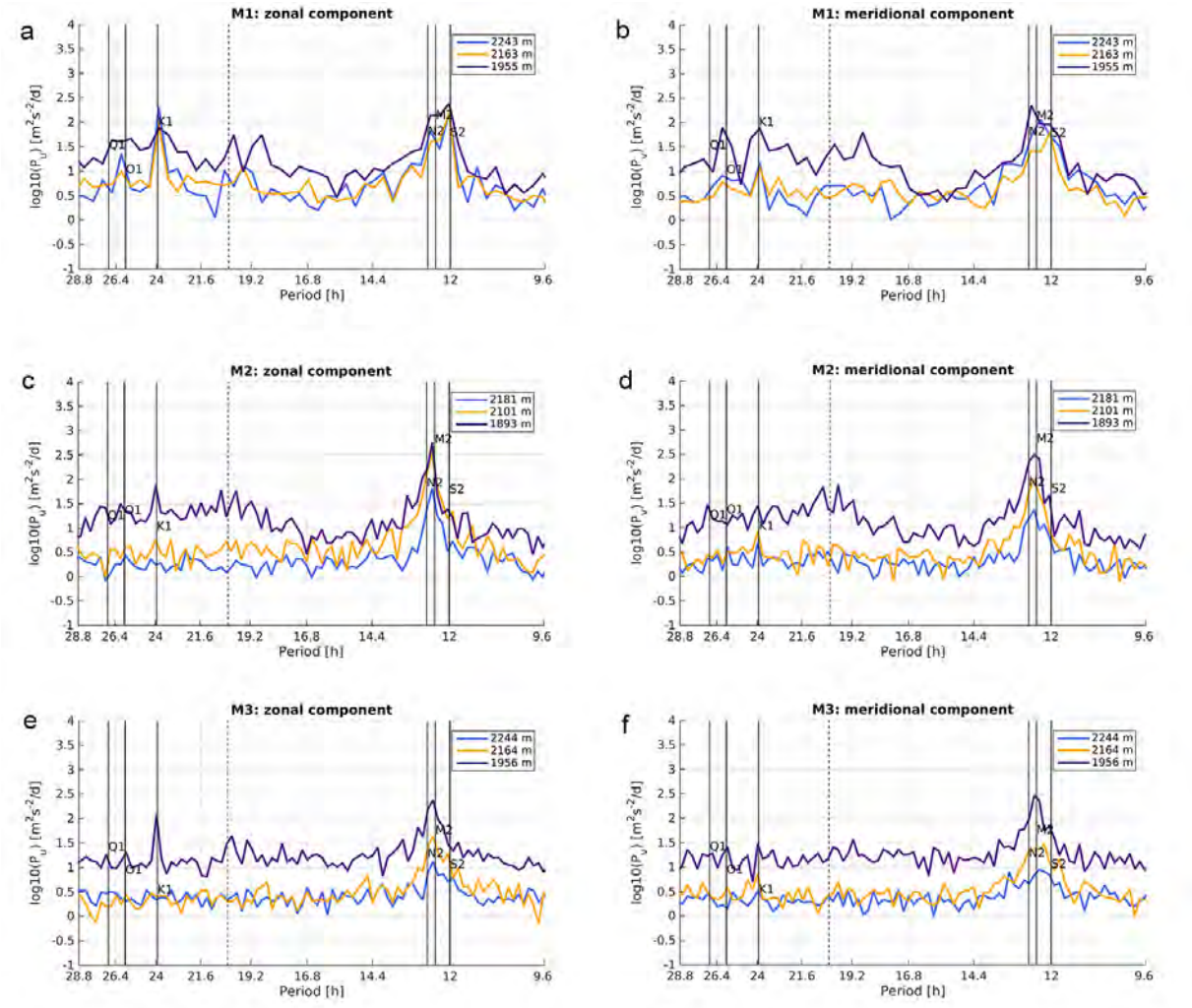

Figure 11: Same as Figure 10, but zoomed between 9 to 29 h.

Is this K1 tidal component enhancement occurring throughout the whole time series, or is it limited to a time window within the time series? To answer this question, we performed a wavelet analysis of the

two components of the velocity, for near-bottom measurements in M1 (Figure 13a and b), and in M2 (Figure 13c and d) for comparison. In Figure 13 the power spectrum (y-axis and colour) is shown as it develops through time (x-axis), revealing that the K1 tidal component enhancement of the zonal component in M1 (Figure 13a) is mostly taking place in the first half of the record (June 2014 to September 2014), while in the second half of the time series the spectrum resembles a "regular" spectrum, such as that at M2 (Figure 13c). However, in November 2014 another isolated event of K1 enhancement is observed. No signature of these enhancement events is visible in the meridional component of the velocity at the same location (Figure 13b), nor in both components at M2 (Figure 13c and d).

In general, however, both diurnal and semidiurnal tidal components appear to be more powerful at the M1 location than at M2 location.

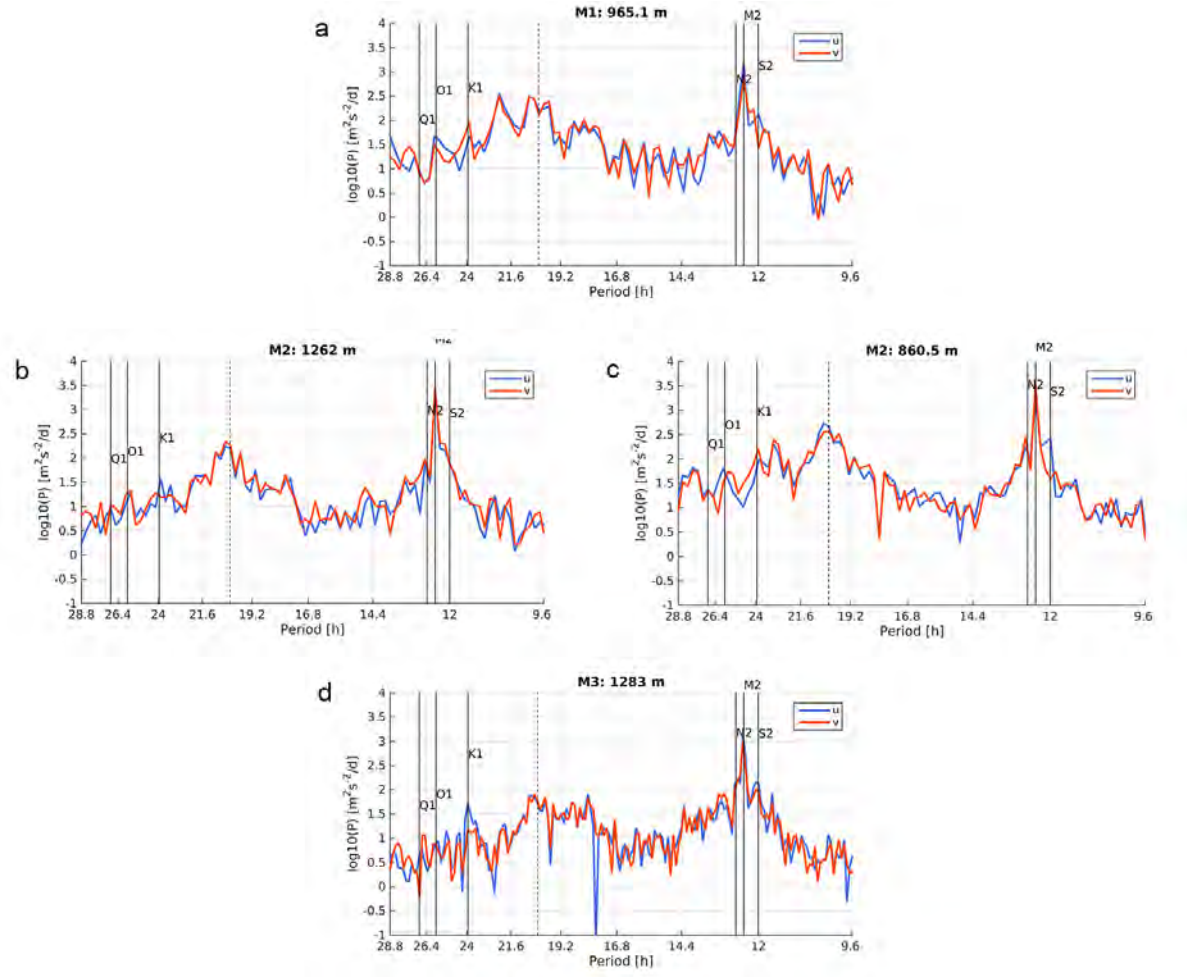

Figure 12: Same as Figure 11, but for the two components of the velocity measured by the four moored current meters.

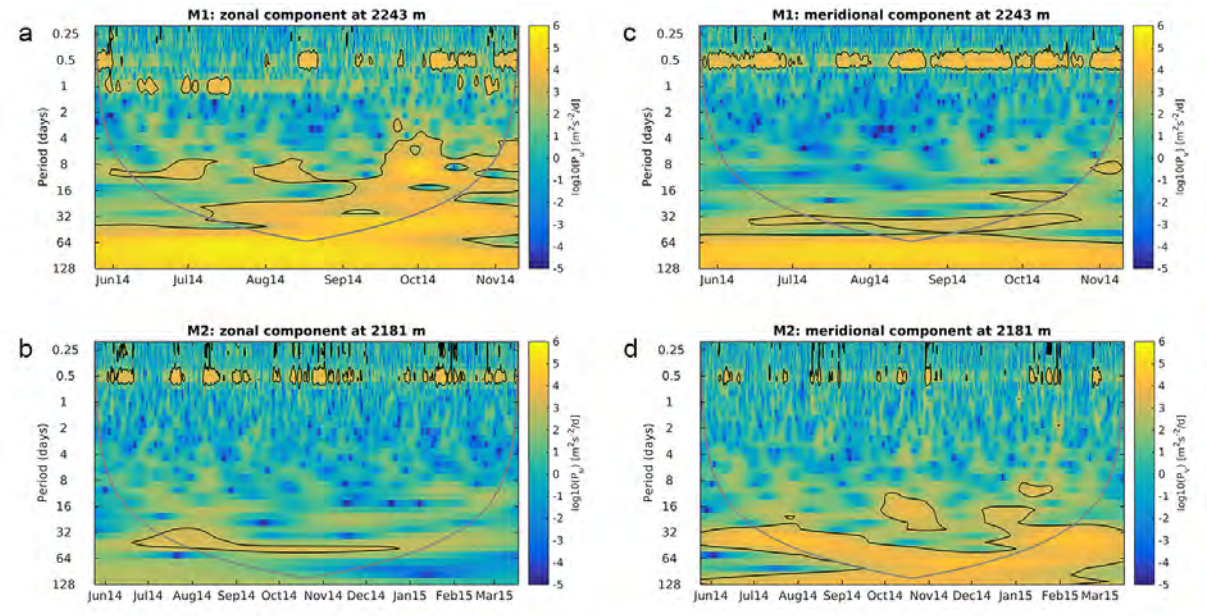

Figure 13: Wavelet analysis for the near-bottom zonal (left) and meridional (right) component at M1 (a,b) and M2 (c,d). Signals are the same as in Figure 10. Gray line corresponds to the so-called cone-of-influence (Torrence and Compo, 1998), black lines correspond to 95% significance contour.

c) Mean flow

Using the velocity time series, we can now consider the mean and extreme current values characterising the Rainbow area. Time averaged values and directions are presented in Figure 14a. Brown colours represent ADCP measurements: dark brown for the near-bottom currents, medium and light brown for shallower measurements, for the same depth intervals as in Figure 10. Note that at M3 they all almost superpose, and at M2, the near-bottom current is almost covered by the mid-depth ADCP measurements. Blue colours represent current meter averaged values and directions: dark blue for measurements below 1000 m, light blue for measurements above 1000 m. For comparison, in Figure 14b, from Thurnherr and Richards (2001), a similar sketch of the mean flow regime is reported, using measurements from a single cruise in 1997. In Figure 14b, solid arrows represent the flow below 2000 m; dashed line indicates the region where enhanced mixing is expected; white arrows represent the flow above 2000 m.

With the new long time series available, we can confirm that the deep, near-bottom layer, hydraulically and topographically controlled, is separated from the layer above (above 2000 m, in Thurnherr and Richards (2001)'s definition), as is clear from its different spectral content (see Figure 11). Its behaviour seems to be quite robust through time, since the flow pattern is quite close to 1997 expectations (Thurnherr and Richards, 2001), including the re-circulation patterns in the north-east of the Rainbow hill.

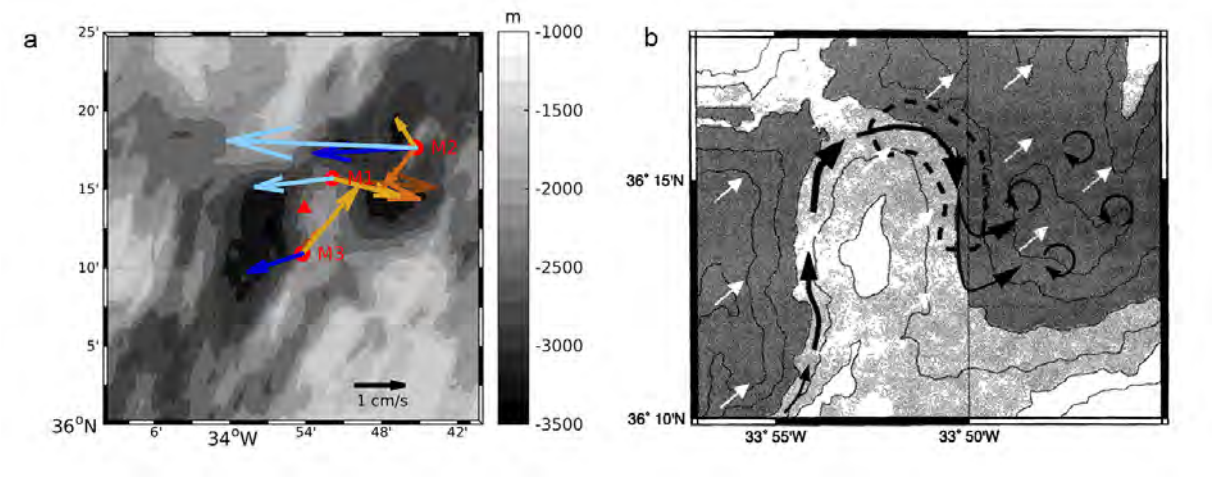

Figure 14: a) Mean flow around the Rainbow Ridge from mooring measurements. Brown, orange and yellow colours represent ADCP measurements: brown for the near-bottom currents, orange and yellow for shallower measurements, same depth intervals as in Figure 10. Blue colours represent current meter measurements: dark blue for measurements below 1000 m, light blue for measurements above 1000 m. b) Sketch of the mean flow regime from Thurnherr and Richards (2001). Solid arrows represent the hydraulically controlled flow below 2000m; dashed line indicates the region where enhanced mixing is expected; open arrows represent the flow above 2000 m.

However now, thanks to the shallower current meter measurements (around 1000 m), we can also distinguish a shallower layer, that on average is moving westward, in accordance with the general circulation within a sub-tropic gyre. As we have seen from Figure 9, we can also distinguish between measurements above and below 1000 m that seems to be affected by different processes. It will be interesting to compare these layers, obtained by hydrodynamic information only, and the corresponding hydrographic structure of the basin. This would be illuminating in terms of vertical transport of material, relevant for understanding and predicting the horizontal and vertical spreading of the existing and future plumes in the canyon.

Maximum values of current magnitude are also obtained from the time series and presented in Figure 15 at different depths at the three mooring locations. Maximum horizontal near-bottom observed values (Figure 15a) are similar in the three mooring locations, about 0.15-0.18 m/s, and comparable with literature (Thurnherr and Richards, 2001). In the upper part of the ADCP measurements, the maximum value for horizontal velocity at M3 stands out (0.5 m/s against 0.2-0.3 m/s at M1 and M2). This is due to the strong event happening in October 2014 (see Figure 8e and f). Enhanced values at about 200 to 300 m from the bottom with current values around 0.25 cm/s were also observed in the 1997 data set (Thurnherr and Richards, 2001), suggesting that this might be a permanent feature in the region. In the upper layers, the maximum recorded values are again comparable among the three locations, around 0.2-0.3 m/s. These relatively high current values are indicative of a very energetic near-bottom environment and are of key importance for planning and performing seabed operations in this area. For this, we also plot the observed maximum values for the vertical component of the velocity (Figure 15b). Note that the current meter measurements at M3 was an Aanderaa, therefore vertical velocities at this depth are not available. Maximum values for vertical velocity go from about 0.04 m/s in the near-bottom layer to 0.08 m/s for the higher layers. Again, values at the three locations are similar.

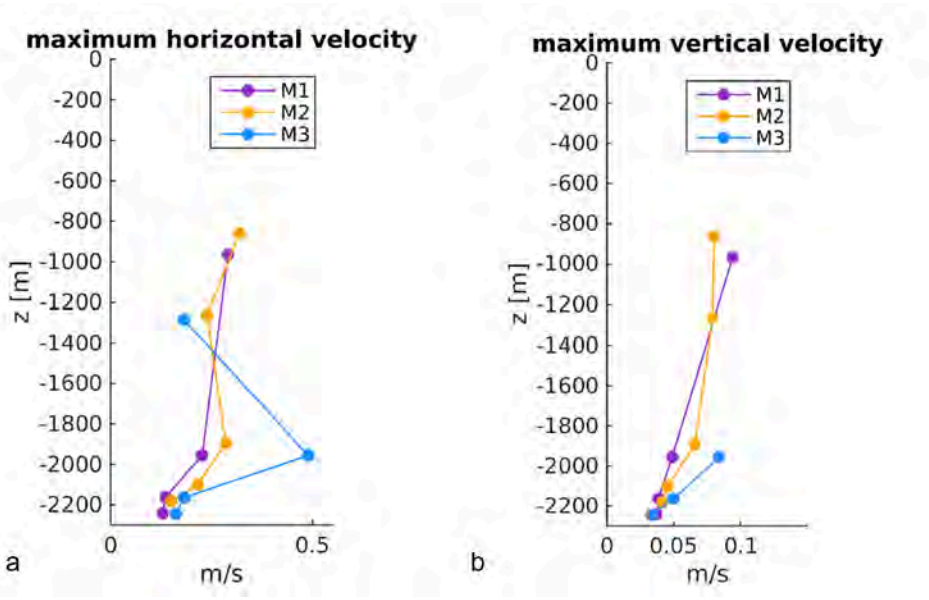

Figure 15: Maximum values of current magnitude recorded at different depths from ADCPs and current meters. Left: horizontal current maximum values; right: vertical current maximum values.

3. Site 2: Lucky Strike hydrothermal vent field (MAR)

The Lucky Strike hydrothermal vent field is located on a seamount in the MAR Rift Valley, at 32º 17' W, 37º 18'N, SW of the Azores Triple Junction (Figure 1b and 16). This segment of the Rift Valley is located inside the Portuguese Exclusive Economic Zone (EEZ). The field is at an average depth of 1700 m. Multiple hydrothermal vents occur over an area of about 300 m x 700 m, and inject plumes at different temperatures, going from 200-212ºC up to 333ºC (Langmuir et al., 1997; Thurnherr et al., 2008).

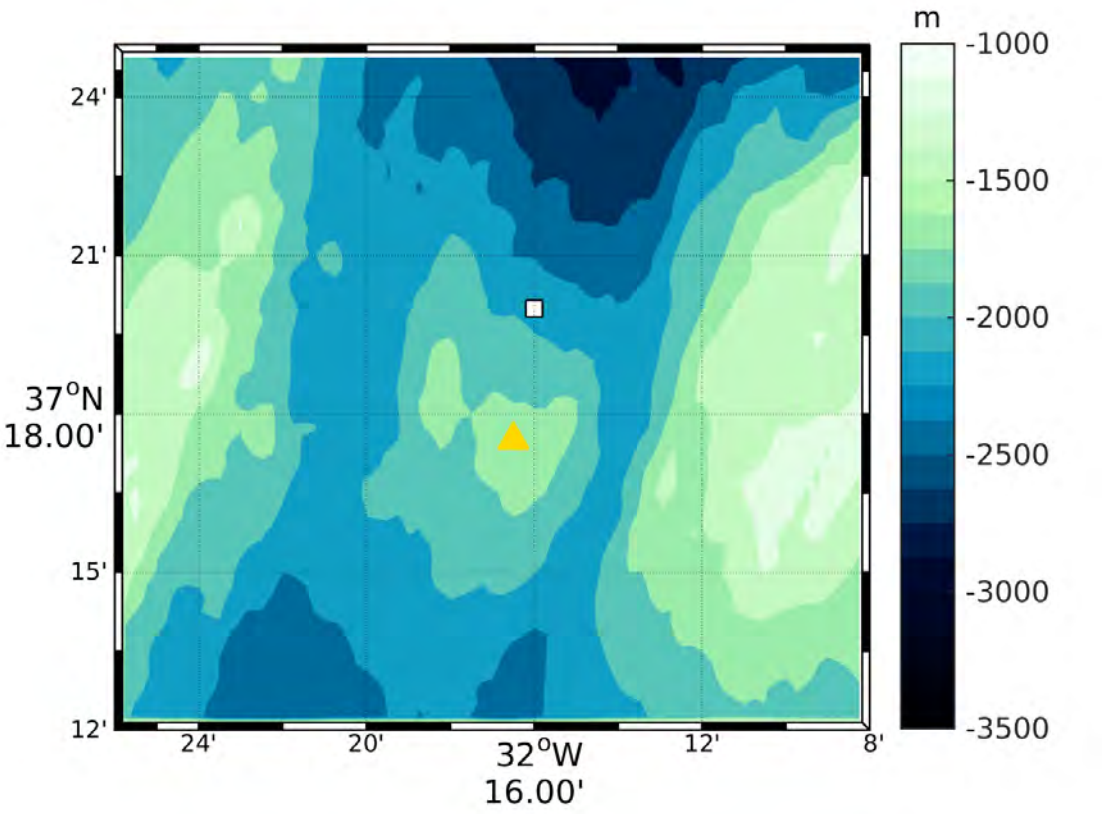

Figure 16 Bathymetric map of Lucky Strike area. The hydrothermal vent field is marked with the yellow triangle. The white square indicates the position of the 13 h of CTD/LADCP continuous measurements.

Main literature references for this site are Aleynik and Lukashin (2005); German et al. (1996a, 2008); Langmuir et al. (1997); St. Laurent and Thurnherr (2007), and Thurnherr et al. (2008). For hydrography only see also Tippenhauer et al. (2015); Wilson et al. (1995, 1996).

3.1 Data, instruments and methods

The data set presented in this report was collected during the 64PE388 cruise in May 2014 with RV Pelagia, on the way to the Rainbow field area. The instrumentation and methodology used in this site is exactly the same as used in the Rainbow area (described in Section 2.1). In the Lucky Strike area, however, only a 13h CTD/LADCP station was performed (white square in Figure 16) in the area north of the vent field to assess the hydrographic and hydrodynamic variability of the site on the tidal timescale. The whole water column was sampled in the 10 acquired profiles.

3.2 Results and discussion

a) Tidal variability of currents

Analogously to measurements Rainbow vent field, local tidal variability has been assessed thanks to a 13-hour CTD/LADCP yo-yo station (10 casts in total). The hydrographic and current measurements were performed at about 4.5 km north of the Lucky Strike vent field in the along-channel direction, between approximately 5 m from the surface to 20 m above the bottom, at about 2050m. Current

speed and direction, averaged in four depth layers (1000-1250 m, 1250-1500 m, 1500-1750 m, and 1750 m to bottom) are presented in Figure 17. As in Figure 7, the colour of the arrows represents time, and goes from red to yellow. The first cast started on 12 May 2014 08:16 UTC, and the last cast started on 12 May 2014 20:14 UTC. A thin, black arrow is superimposed on the colour arrow if the particle plume originated by the Rainbow hydrothermal vent field is observed, using the same instrumentation described in section 2.2.2. In the bottom panel of Figure 17, the local barotropic tidal ellipse is shown, as obtained using the FES2012 model (Carrére et al., 2012) for the same time frame. Time colour code is the same as in the other panels.

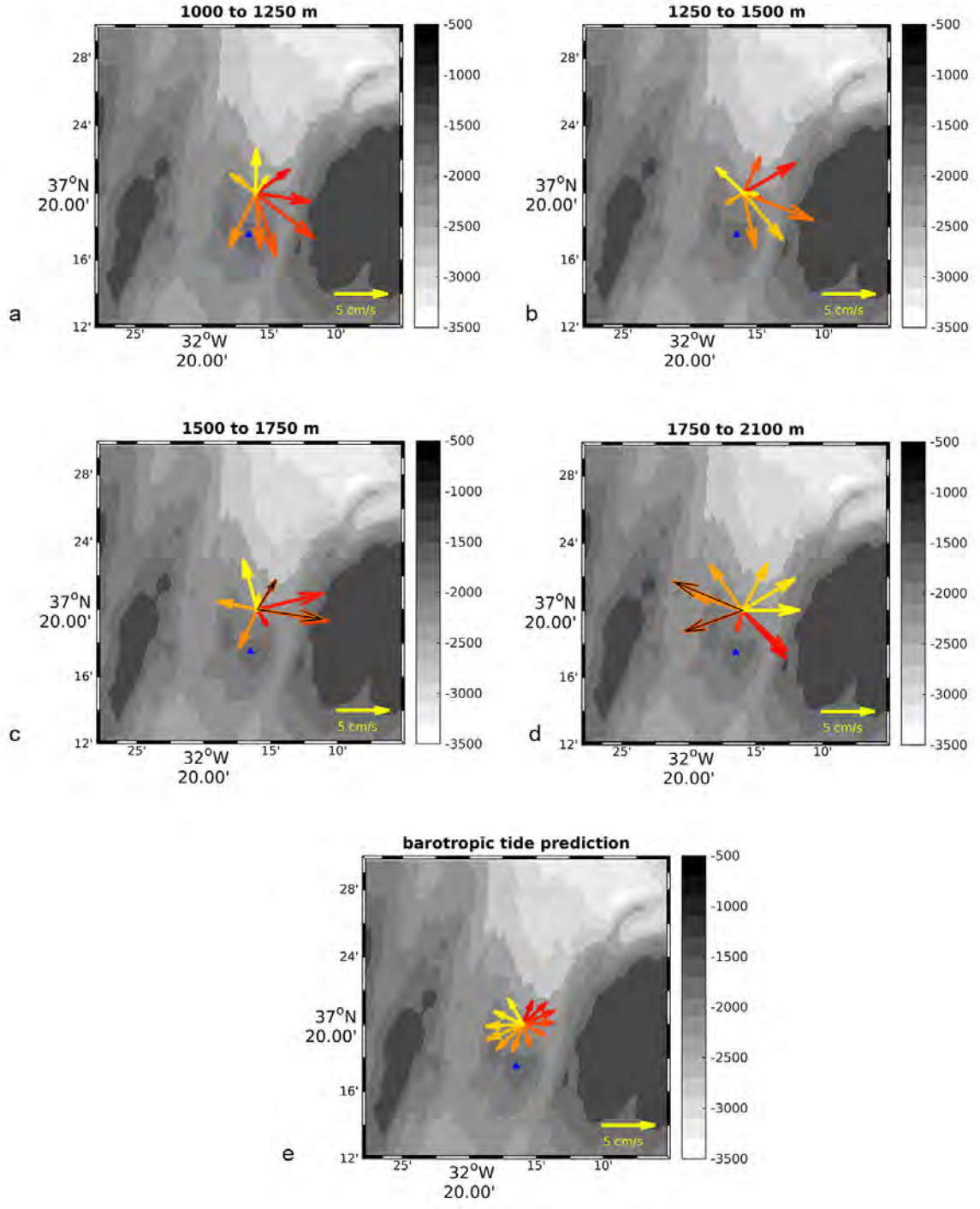

Figure 17 (previous page): a-d) Top to bottom, left to right, current speed and direction as measured by the LADCP averaged in four depth layers, according to each panel title. Colour of the arrows represents time, from red to yellow. First cast started on the 12th of May 2014 08:16 UTC, last cast started on the 12th of May 2014 20:14 UTC. A thin black arrow is superposed on the colour arrow when the plume is detected using turbidity measurements. e) The local barotropic tidal ellipse as obtained using the FES2012 model (Carrére et al., 2012) for the same time frame. Time colour code is the same as in the other panels. The blue triangle marks the position of the Lucky Strike vent field.

A big difference is observed when the 13 h measurements performed in the Lucky Strike area are compared to the ones performed in the Rainbow area (section 2.2.2). Here, the tidal ellipse is visible throughout the whole water column since local topography does not prevent the current to flow in any particular direction. Although an anticyclonic (clockwise) tidal ellipse is visible in all layers, differences are present between measured velocities and the modelled barotropic tide. In terms of current magnitude, values in the Lucky Strike area are closer to expected model values than in the Rainbow area, although cross-channel flow appears to be largely underestimated by the model. Near bottom velocity magnitudes are of the order of 0.05-0.1 m/s, as expected from previous measurements in the area (Thurnherr et al., 2008). However, no bottom enhancement of the current in a particular direction was observed here, at any time during the measurements.

The phase of the three layers down to 1750 m agrees with the barotropic model, whilst it appears shifted by about 90 degrees in the near-bottom layer. As suggested by Thurnherr et al. (2008), the flow is hydraulically controlled around the Lucky Strike seamount only up to 1800 m. This, as in the Rainbow case, is suggestive of barotropic to baroclinic tide conversion due to current-topography interactions. The fact that we are able to capture the whole tidal ellipse, with no current direction restriction due to topography suggests that we can consider our measurement location as representative of the dynamics happening in the middle of the ridge axis and on top of the sea mount. Thurnherr et al. (2008) observed that there is no really coherent circulation over the Lucky Strike seamount, which is in contrast to observations in the west and east passage. In the latter, for example, there is a strong prevalence of northward flow, measured both by one-year long moored ADCPs and with spatially distributed LADCP profiles (Thurnherr et al., 2008). The centre of the seamount was indeed described in Thurnherr et al. (2008) as tidally dominated, with the same probability of currents going northward and southward, as it is the case for our 13 h measurements.

The presence or absence of the hydrothermal plume is puzzling in both the Lucky Strike area and the Rainbow area, although perhaps for slightly different reasons. The plume is observed in only two casts out of 10 (the 4th and the 5th, between 12 and 14 UTC of 12 May), below 1650 m. The puzzling aspect comes from the fact that from the layer 1500-1750 m to the layer 1750 m to bottom is strongly sheared. The current direction at these times changes dramatically from east/north-east to west/ south-west, without loosing the plume particle. Accurate hydrographic investigation is needed to check whether the currents, although reversing their direction, are able to transport a specific water mass and its particle content through these two vertical layers. Moreover, currents that at different times present the same spatial direction and magnitude of the 4th and 5th casts in the two deepest layers (see for example the last measurements, bright yellow arrow, in the near-bottom layer in Figure 17), do not show any trace of the plume, at least in turbidity. Could this also be explained by intermittent plume emission? Unfortunately, we have no information on this. It is known (Thurnherr et al., 2008) that plume traces from multiple sources can be detected at Lucky Strike. Enhanced turbidity in the layer 1500-1750 m (Figure 17c) is usually associated with known Lucky Strike vents, implying a plume rise of about 100 m during the survey (comparable to that found in Thurnherr et al., 2008). The deeper plume (Figure 17d) is usually associated with another, unknown hydrothermal source, located south of the Lucky Strike volcano. This does not fit with the observation of this deep plume during west/southwest currents. However, as we have seen at our yo-yo station location, tidal effects are predominant, and they might be able to temporarily reverse the mean northward flux expected within the canyon.

4. Site 3: Clarion-Clipperton Zone polymetallic nodule deposits

Polymetallic (or manganese) nodules are blackish-brown, irregular to round concretions with diameters of about 1 to 6 cm. They are found in deep-sea abyssal plains (between 4500 and 6000 m) and form due to the precipitation of manganese and iron oxides as well as numerous other major and trace metals from sea water and the pore waters of the sediment. Economically relevant metals contained in the nodules are copper, nickel and cobalt. Growth rates are extremely low, with values varying between about 2 and 100 mm/Ma. The largest and most important deposits are found in the NE Pacific, in the so-called manganese nodule belt in the Clarion and Clipperton fracture zones - CCZ (Figure 1). The CCZ has the largest known concentrations of high-grade polymetallic nodules: about 50% of the sediment surface is covered by manganese nodules, which potentially have great commercial value.

In this area, the International Seabed Authority (ISA) has granted 12 licenses for the exploration of manganese nodule fields. Several countries currently hold exploration license areas in the CCZ (Figure 18). In addition, the regional management plan of the ISA established also 9 "Areas of Particular Environmental Interest" (Figure 18) for the protection and preservation of the marine environment and its biodiversity. It appears, however, that large portions of these areas have never been visited by scientific cruises, and the information about both their ecosystems and their hydrodynamic and hydrographic characteristics are mostly unknown. For the moment, it is thought that the scale of impacts that would be associated with nodule mining in the CCZ may affect 100s to 1000s of km^2 per mining operation per year, depending on different local conditions.

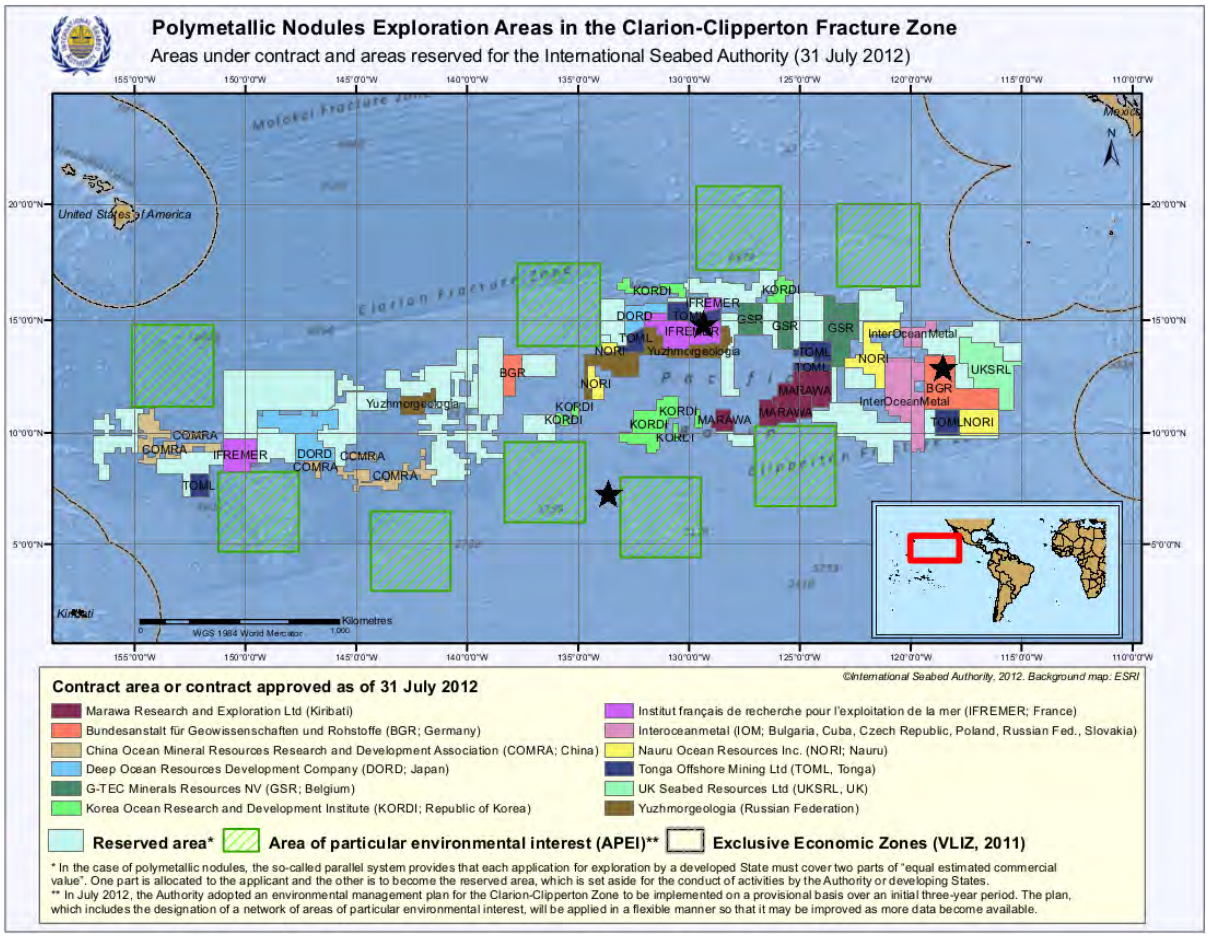

Figure 18 License Areas, Reserved Areas and Areas of Particular Environmental Interest in the CCZ as designated by the ISA. The three black stars represent the three sites described later in the section.

Estimating these conditions and the consequent size of impacted area is one of the aims of the MIDAS project. However, another scientific project, focused only on the CCZ and on polymetallic nodule deposits, has recently started within the context of the Joint Programming Initiative Healthy and Productive Seas and Oceans (JPI Oceans). The project is a JPIO Pilot Action on "Ecological aspects of deep-sea mining", running for three years from January 2015.

Several partners and ocean surveys relative to the two projects overlap, and thus new observational data on the CCZ area will be available in the near future, hopefully including relatively long term current observations, as well as long-term hydrographic data for the area. For the moment, we can rely on published information to get a general picture of the hydrodynamic regimes in the CCZ area. For this site, literature references are Johnson (1972); Kontar and Sokov (1994). The relevant extraction from the cruise reports for the MANAGAN-2013/2014 cruises in the East BGR area have been kindly provided by Annemiek Vink (BGR, Bundesanstalt für Geowissenschaften und Rohstoffe).

4.1 Measurements around 7º40'N, 134ºW (1972)

Hydrodynamic information on this area is reported in Johnson (1972). A series of four current meters was moored at the height of 5 to 25 m above the bottom, measuring velocities for a period of about four days. The observations have been acquired in order to follow the circulation and fate of the bottom water in the North Pacific. The bottom water is supposed to enter the North Pacific through a narrow passage northeast of Samoa. Prominent topographic features such as the Hawaiian Ridge, Line Islands Ridge, and Mid-Pacific Mountains serve then as major barriers to bottom water flow, and its spreading eastward towards the CCZ is not very well defined, due to the scarcity of measurements and to the extremely small gradients of bottom potential temperature that do not allow a unique determination of the flow direction.

The observed current speeds were generally low, less than 0.1 m/s, during the period of observation, but fluctuated significantly because of tidal effects. During the period of observation, the semidiurnal signal was the most energetic tidal component. However, even if the tidal modulation was strong in the velocity magnitude, the direction of the flow at the different mooring locations was remarkably uniform, despite the distances between the moorings, going from 2 up to 15 km.

On the plateau, mainly eastward-flowing currents were recorded, whereas in the depression to the west of the plateau instruments recorded a north-eastward flow. The data thus suggest that in this area there is a net regional transport of bottom water toward the east, with minor modifications in direction due to local topographic effects.

4.2 Measurements from 12-16ºN, 129-133ºW (1984-1990)

Hydrodynamic information for this area is reported in Kontar and Sokov (1994). This region of the Clarion Clipperton Zone is an undulating abyssal plain consisting of abyssal hills 100 to 1000 m in height with occasional seamounts up to 1000 to 2000m high. Previous hydrographic characteristics (Mantyla and Reid, 1983) had suggested a general north-easterly flow in the area, however current observations in Kontar and Sokov (1994) do not support this interpretation. In fact, bottom currents in the region appear to vary greatly in both velocity and direction. Bottom currents are generally weak with average velocities of about 0.02 to 0.06 m/s (Hayes, 1979, 1980), but these average velocities have been found to be statistically unreliable because of the strong temporal variability. 50 to 80% of the total variation is explained with periods exceeding 30 days, while, in the high-frequency part of the spectrum, the variation is predominantly tidal (semidiurnal) and inertial ($f = 2\Omega \sin \phi \approx 48$ h) (Hayes,

1979). Bottom currents in the region characteristically have a high vertical coherence in the near bottom 500 m, regarding both fast and slow variability. A bottom intensification of velocity over the benthic boundary layer (BBL) is also observed, a feature similar to other regions in the world ocean. Velocity usually increases from 20 to 100 m above the bottom, but decreases further from the bottom. The maximum velocity level is well correlated with the upper boundary of the Ekman bottom turbulent layer, i.e. intensification is observed above the BBL.

In measurements reported by Kontar and Sokov (1994), bottom currents in the north-eastern tropical Pacific have been also observed to be predominantly weak (0.02-0.03 m/s), but the flow was characterised by the alternation of stronger, quasi-unidirectional currents (0.1-0.3 m/s) and periods of slower motions. The predominant direction was SW-W, but very little coherency in current direction was observed between neighbouring moored instrumentation during the period of slow motion.

Events of strong near-bottom currents, often referred to as "benthic storms", are generally recognised for their high coherency in bottom current direction at all points of measurements (despite locations being from 36 to 200 km apart in the 1988 experiment). They are characterised by a sharp change in the direction of the current to the opposite direction, accompanied by a sharp increase in velocity magnitude.

In terms of spatial extent, benthic storms have been thus associated with large-scale process, in particular deep-reaching, anticyclonic eddies. In the period 1984-1990, eddies were also traced by monitoring the maximum sea-height variability. The excess of eddy kinetic energy at the surface was apparently transmitted to the seafloor to water depths as deep as 4500-4750 m (the depths of the current meters in Kontar and Sokov (1994) 1986 experiment). In the region, the oceans therefore appear to be "stiff" with respect to large-scale motions, and the ultimate cause of benthic storms was associated with the storage and vertical transmission of eddy kinetic energy from the top of the ocean to the deep seafloor. The data from north-eastern tropical Pacific in Kontar and Sokov (1994) appear thus to be virtually depth-independent and, combined with shallower current measurements acquired at the same time, show that the benthic storms are not confined to the near-bottom but fill the whole water column.

While in the 1986 and 1988 time series benthic storms were observed due to the passage of anticyclonic eddies with typical southward currents intensified near the bottom, in the 1989 time series a cyclonic eddy has been traced down to the near bottom current, associated to a quasi steady N-NE or N-NW direction for almost 2 months. In this case, only a small intensification of bottom currents was observed (no evident benthic storm), but the coherency of the direction of the currents agreed entirely with the measured and estimated current direction at the overlying waters, and thus the north-flowing bottom current are likely to be due to the extension of the cyclonic eddy all the way to the bottom.

4.3 Measurements from the Eastern BGR license area (2013-2014)

Three long-term moorings equipped with current and turbidity profilers were deployed as close to the seafloor as possible in the eastern BGR license area (see Figure 18) for approximately 1 year between April 2013 and May 2014, sampling at 1h time resolution. The aim has been to collect data on current variability in the lower 30 m near the bottom, close to the manganese nodule fields present in the area.

Vertical profiles from ADCPs have been averaged in order to obtain an averaged current speed and direction in this water layer. The three ADCPs, positioned about 10 km from each other (see Figure 19), show similar distributions of current directions and magnitudes. Current speeds in the water layer

10 - 17.5 m above the seafloor range between 0.002 and 0.5 m/s for the lowest values and between 0.11 to 0.13 m/s for the maximum values, most likely varying because of small, local topographic differences. The average speed over the 13-month measurement period was about 0.037-0.04 m/s for all the three locations. A single event of strong current speed and predominantly eastward current flow characterises May 2013 and it is visible in the time series relative to all three locations, with measured current values up to 0.14 m/s. This event has been described in detail in Inall et al. (2015), where it is associated with the westward propagating "super-eddy", resulting from the merging of two eddies: one originating from eastern Mexico and the other via the Papagayo gap-winds of Nicaragua. Sea surface velocities derived from satellite data and near bed velocities at all three sites clearly show the influence of the eddy. Surface velocities peaked at 0.40 m/s, while near bed velocities at 0.14 m/s, lagging in time by 10 days or more.

In general, as shown in Figure 19, a E-SE current direction predominates, with the strongest currents (> 0.08 m/s) always flowing in the E-SE direction; a N-NW current direction is rare. Spectral analysis of the time series in the Eastern BGR area indicates a clear 12.4-hour tidal cycle with amplitudes of several cm/s as well as strong 27-day lunar cycle.

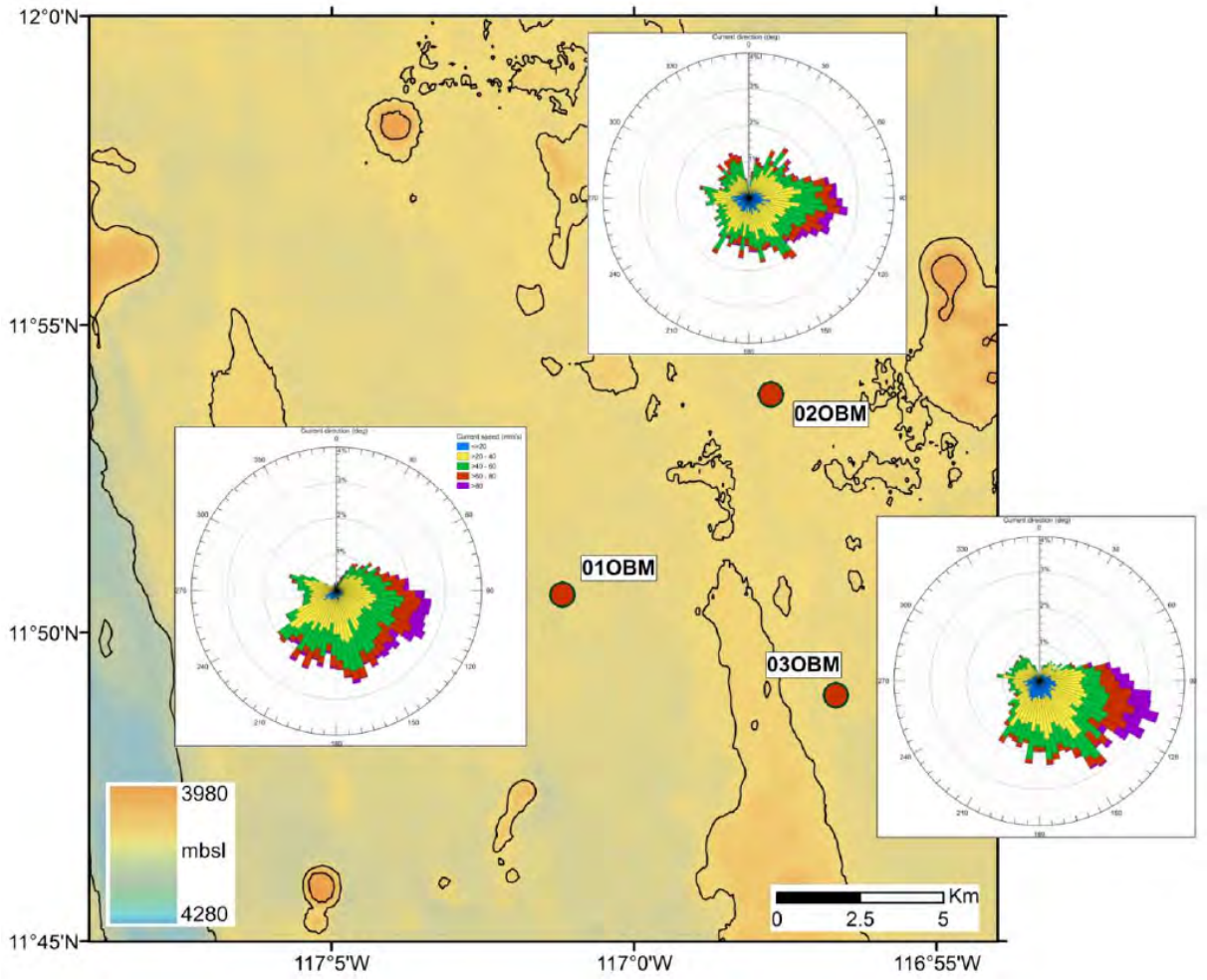

Figure 19 Radial plots of current speeds and directions in the water layer 10 - 17.5 m above the sea floor at the three OBM sites from April 2013 to May 2014 plotted as a function of their frequency of occurrence in relation to topography. Data and Figure from MANGAN 2014 cruise report (from Annemiek Vink, BGR).

5. Conclusions and implications for deep-sea mining

The goal of hydrodynamic (as well as hydrographic) characterisation of a site in the context of deep-sea mining is the understanding and - possibly - the prediction of the final spatial distribution of a sediment plume. This knowledge is crucial in order to foresee the physical, biological and ecological consequences of mining activities, and thus enabling the interested parties in planning operations that will be environmentally feasible and safe. However, going from observations to predictions, given also the use of dedicated numerical models (see for example Aleynik et al. (2015)), is not an easy task. The horizontal and vertical spreading of a natural and/or artificial (mining) plume is determined by processes involving a wide range of different temporal and spatial scales, from minutes to seasons, from centimetres to kilometres. For this reason, a complete and detailed characterisation of three sites, accounting for all relevant phenomena, is unrealistic given the project time and resource constraints, and falls far beyond the scope of this report. Here we have limited ourselves to the description of the hydrodynamic data sets collected within the MIDAS project on two neighbouring sites on the MAR (sections 2 and 3). For the Pacific site (Section 4) we have relied on a literature review. In particular, we have been interested in those processes that could potentially lead to increased turbulence or current speeds, with consequent enhanced horizontal spreading of the mine tailings material or injections of material into the upper parts of the water column.

Regarding the two sites on the MAR (sections 2 and 3), for which we have the largest availability of in situ data, including newly acquired time series of velocity, relevant site-specific processes are mainly shaped by the sharp topography of the area. In the Rainbow area, the velocity phase shifts throughout the water column (see Figure 7) are indicative of a very active internal wave field, most likely resulting from barotropic to baroclinic tide conversion due to interactions between currents and local topography. Estimation of vertical diffusivity will quantify the local vertical mixing properties induced by propagating (or even breaking) internal waves in the region and their uneven spatial variability, mainly in the near bottom layers but not exclusively. An understanding and realistic estimation of this parameter are crucial in order to obtain realistic results from modelling experiments. With these new observations, for example, we can exclude a major role of (vertical) mixing due to breaking of near-inertial waves in the bottom layers, hypothesised in Thurnherr (2006), and from the spectral analysis in Figure 11, near-inertial frequencies appear to be much less energetic than tidal frequencies.

We have observed that the local topography can also be responsible for trapping of waves of certain frequencies. An example of this is recorded in the Rainbow area, where a local near-bottom enhancement of the K1 tidal component is observed in the zonal component at only one of the mooring locations (Figure 11a), and in a specific time window (Figure 13a). This feature is not captured by near-field, high-resolution models (Aleynik 2015, personal communication), and it exemplifies the value of in situ observations in such a complex deep-sea environment.

We are able to observe the prominent role of topography at the Lucky Strike location, despite only having hydrodynamic information over a single tidal cycle (Figure 17). This is particularly evident when our measurements, located north of the Lucky Strike seamount, are compared to literature results from neighbouring locations, but in the east or west passage.

As a last comment on the MAR sites, a distinct dynamic is observed at different depth layers (below and above 2000 m, but also below and above 1000 m; see Figures 6, 7 and 9). Surface or intermediate forcing, such as a possible passage of a meddy (Mediterranean-eddy), seems thus not to influence the near bottom currents, perhaps because of the steep flanks of the canyon characterising this region, and isolating the shallower from the deeper dynamics.

This appears to be a major difference with the near bed dynamics in the CCZ sites described in Section 4. In this area the passage of an eddy and its influence on the whole water column dynamics

down to the near bottom layers seems to be a common feature. The induced "benthic storms" clearly have consequences on, for example, the peak velocities found in the near bottom environment, and should certainly to be taken into account in the design of any kind of deep sea operations.

Any activities at any deep-sea site will undeniably affect the status of the existing environment, at the seafloor, in the near bottom layers, as well as in at least a portion of the overlying water column. Particle plumes will likely be created at the seabed by the underwater machinery and tailing plumes will be most likely re-introduced in the water column after the processing of the material at the sea surface. Obviously, the re-settling of these newly introduced sediment particles will impact areas of the seafloor that are well beyond the boundaries of the mined area. To be able to predict the size of this impacted area, knowledge of the state of the mining site before any mining operations is crucial. In this report, we have seen that in situ observations provide the basis of the characterisation of specific sites. Observations must be carried out in the near field of a site, as well as in the far field, to be able to place the region of interest in a larger basin-scale context. Satellite data can be also used in combination with in situ observations, to study the influence of surface or intermediate forcings on near bottom dynamics. Time series of current measurements, possibly at least one year long, are also very important to assess both the local current field amplitude values and directions, its spectral content and its modulation throughout the seasons. This information, in combination with the known seasonality of biological processes, is essential in understanding the types of ecological impact of underwater operations, and the resilience and natural recovery potential of neighbouring deep-sea communities, whether connected or not by the near bed flow.

6. References

Aleynik, D., Dale, A. C., and Inall, M. E. (2015). Near-field hydrodynamic modelling of two case study sites. MIDAS deliverable 2.2.

Aleynik, D. L. and Lukashin, V. N. (2005). Hydrothermal plume dynamics at MAR sites - direct observations. InterRidge News, 14, 19-22.

Carrére, L., Lyard, F., Cancet, M., Guillot, A., and Roblou, L. (2012). Fes 2012: a new global tidal model taking advantage of nearly 20 years of altimetry. Proceedings of 20 years of Altimetry, Venice 2012.

Cave, R. R., German, C. R., Thomson, J., and Nesbitt, R. W. (2002). Fluxes to sediments underlying the Rainbow hydrothermal plume at 36°14'N on the Mid- Atlantic Ridge. Geochimica et Cosmochimica Acta, 66(11), 1905-1923.

Dale, A. C. and Inall, M. E. (2015). Categorisation of deep sea sites according to the effect of local hydrodynamics on the near-field dilution of mining discharges. MIDAS deliverable 2.1.

Dymant, J., Bissessur, D., Bucas, K., Cue_-Gauchard, V., Durand, L., and Fouquet, Y. (2009). Detailed investigation of hydrothermal site Rainbow, Mid-Atlantic Ridge, 36 13'N: Cruise MoMARDream. InterRidge News, 18, 22-24.

Egbert, G. D. and Erofeeva, S. Y. (2002). Efficient Inverse Modeling of Barotropic Ocean Tides. Journal of Atmospheric and Oceanic Technology, 19, 183-204.

German, C. R., Parson, L., HEAT Scienti_c Team, Bougault, H., Coller, D., Critchley, M., Dapoigny, a., Day, C., Eardley, D., Fearn, a., Flewellen, C., Kirk, R., Klinkhammer, G., Landure, J.-Y., Ludford, E.,

Miranda, M., Needham, H., Patching, J., Pearce, R., Pelle, H., Radford-Knoery, J., Rouse, I., Scott, J., Sto_regen, P., Taylor, P., Teare, D., and Wynar, J. (1996a). Hydrothermal exploration near the Azores Triple Junction: tectonic control of venting at slow-spreading ridges? Earth and Planetary Science Letters, 138(1-4), 93-104.

German, C. R., Klinkhammer, G. P., and Rudnicki, M. D. (1996b). The Rainbow hydrothermal plume, 36º15'N, MAR. Geophysical Research Letters, 23(21), 2979-2982.

German, C. R., Richards, K. J., Rudnicki, M., Lam, M., and Charlou, J. (1998). Topographic control of a dispersing hydrothermal plume. Earth and Planetary Science Letters, 156(June 1997), 267-273.

German, C. R., Bennett, S. a., Connelly, D. P., Evans, a. J., Murton, B. J., Parson, L. M., Prien, R. D., Ramirez-Llodra, E., Jakuba, M., Shank, T. M., Yoerger, D. R., Baker, E. T., Walker, S. L., and Nakamura, K. (2008). Hydrothermal activity on the southern Mid-Atlantic Ridge: Tectonically- and volcanically-controlled venting at 4-5ºS. Earth and Planetary Science Letters, 273(3-4), 332-344.

German, C. R., Thurnherr, a. M., Knoery, J., Charlou, J. L., Jean-Baptiste, P., and Edmonds, H. N. (2010). Heat, volume and chemical fluxes from submarine venting: A synthesis of results from the Rainbow hydrothermal field, 36ºN MAR. Deep-Sea Research Part I: Oceanographic Research Papers, 57(4), 518-527.

Hayes, S. (1979). Benthic current observations at domes sites a, b, and c in the tropical north Pacific ocean. In J. Bischoff and D. Piper, editors, Marine Geology and Oceanography of the Pacific Manganese Nodule Province, volume 9 of Marine Science, pages 83{112. Springer US.

Hayes, S. P. (1980). The bottom boundary layer in the Eastern Tropical Pacific. Journal of Physical Oceanography, 10, 315-329.

Inall, M. E., Aleynik, D., Dale, A. C., and Vink, A. (2015). Central American Gap winds and abyssal CCZ plumes. MIDAS newsletter, Issue 4, Spring 2015.

Johnson, D. A. (1972). Eastward-flowing bottom currents along the Clipperton Fracture Zone. Deep Sea Research and Oceanographic Abstracts, 19(3), 253-257.

Kontar, E. a. and Sokov, A. V. (1994). A benthic storm in the northeastern tropical Pacific over the fields of manganese nodules. Deep Sea Research Part I: Oceanographic Research Papers, 41(7), 1069-1089.

Langmuir, C., Humphris, S., Fornari, D., Van Dover, C. L., Von Damm, K., Tivey, M., Colodner, D., Charlou, J.-L., Desonie, D., Wilson, C., Fouquet, Y., Klinkhammer, G., and Bougault, H. (1997) Hydrothermal vents near a mantle hot spot: the Lucky Strike vent field at 37ºN on the Mid-Atlantic Ridge. Earth and Planetary Science Letters, 148(1-2), 69-91.

Maas, L. R. M. and Zimmerman, J. T. F. (1989). Tide-topography interactions in a stratified shelf sea II. Bottom trapped internal tides and baroclinic residual currents. Geophysical & Astrophysical Fluid Dynamics, 45(1-2), 37-69.

Mantyla, A. W. and Reid, J. L. (1983). Abyssal characteristics of the world ocean waters. Deep Sea Research Part A. Oceanographic Research Papers, 30(8), 805 - 833.

Marshall, J., Adcroft, A., Hill, C., Perelman, L., and Heisey, C. (1997a). A finite-volume, incompressible Navier Stokes model for studies of the ocean on parallel computers. Journal of Geophysical Reasearch, 102, 5753-5766.

Marshall, J., Hill, C., Perelman, L., and Adcroft, A. (1997b). Hydrostatic, quasi-hydrostatic, and nonhydrostatic ocean modeling. Journal of Geophysical Reasearch, 102, 5733-5752.

Percival, D. B. (1993). Spectral analysis for physical applications. Cambridge University Press, Cambridge and New York, USA.

Rabitti, A. and Maas, L. R. M. (2015). Analysis for data requirement for near-field model validation. MIDAS deliverable 2.4.

St. Laurent, L. C. and Thurnherr, A. M. (2007). Intense mixing of lower thermocline water on the crest of the Mid-Atlantic Ridge. Nature, 448 (7154), 680-683.

Thomson, D. (1982). Spectrum estimation and harmonic analysis. Proceedings of the IEEE, 70, 1055-1096.

Thorpe, S. A. (1977). Turbulence and mixing in a Scottish loch. Philosophical Transactions of the Royal Society of London, Series A, Mathematical and Physical Sciences, 286, 125-181.

Thurnherr, A. M. (2006). Diapycnal mixing associated with an overflow in a deep submarine canyon. Deep-Sea Research Part II: Topical Studies in Oceanography, 53(1-2), 194-206.

Thurnherr, A. M. and Richards, K. J. (2001). Hydrography and high temperature heat flux of the Rainbow hydrothermal site (36 deg 14'N, Mid-Atlantic Ridge). Journal of Geophysical Reasearch, 106(c5), 9411-9426.

Thurnherr, A. M., Richards, K. J., German, C. R., Lane-Ser_, G. F., and Speer, K. G. (2002). Flow and Mixing in the Rift Valley of the Mid-Atlantic Ridge. Journal of Physical Oceanography, 32(6), 1763-1778.

Thurnherr, A. M., Reverdin, G., Bouruet-Aubertot, P., St. Laurent, L. C., Vangriesheim, A., and Ballu, V. (2008). Hydrography and flow in the Lucky Strike segment of the Mid-Atlantic Ridge. Journal of Marine Research, 66(3), 347-372.

Tippenhauer, S., Dengler, M., and Kanzow, T. (2015). Turbulence and fine structure in a deep ocean channel with sill overflow on the mid-Atlantic ridge. Deep-Sea Research I, http://dx.doi.org/10.1016/j.dsr.2015.01.001.

Torrence, C. and Compo, G. P. (1998). A Practical Guide to Wavelet Analysis. Bulletin of the American Meteorological Society, 79(1), 61-78.

Wilson, C., Speer, K., Charlou, J.-L., Bougault, H., and Klinkhammer, G. (1995). Hydrography above the Mid-Atlantic Ridge (33-40ºN) and within the Lucky Strike segment. Journal of Geophysical Reasearch, 100(c10), 555-564.

Wilson, C., Charlou, J.-L., Ludford, E., Klinkhammer, G. P., Chin, C., Bougault, H., German, C. R., Speer, K. G., and Palmer, M. R. (1996). Hydrothermal anomalies in the Lucky Strike segment on the Mid-Atlantic Ridge (37º17'N). Earth and Planetary Science Letters, 142(3-4), 467-477.